

First stars

XVI. STIS/HST abundances of heavy-elements in the uranium-rich star CS 31082-001[★]

C. Siqueira Mello Jr.^{1,2}, M. Spite², B. Barbuy¹, F. Spite², E. Caffau^{3,2}, V. Hill⁴, S. Wanajo⁵, F. Primas⁶, B. Plez⁷, R. Cayrel⁸, J. Andersen^{9,10}, B. Nordström⁹, C. Sneden¹¹, T.C. Beers¹², P. Bonifacio², P. François⁸, and P. Molaro¹³

¹ Universidade de São Paulo, IAG, Rua do Matão 1226, Cidade Universitária, São Paulo 05508-900, Brazil

² GEPI, Observatoire de Paris, CNRS, UMR 8111, F-92195 Meudon Cedex, France

³ Zentrum für Astronomie der Universität Heidelberg, Landessternwarte, Königstuhl 12, 69117 Heidelberg, Germany

⁴ Université de Sophia-Antipolis, Observatoire de la Côte d'Azur, CNRS UMR 6202, BP4229, 06304 Nice Cedex 4, France

⁵ National Astronomical Observatory of Japan, 2-21-1 Osawa, Mitaka, Tokyo 181- 8588, Japan

⁶ European Southern Observatory, Karl Schwarzschild Strasse 2, 85748 Garching bei München, Germany

⁷ LUPM, CNRS, UMR 5299, Université de Montpellier II, F-34095 Montpellier Cedex 05, France

⁸ GEPI, Observatoire de Paris, CNRS, UMR 8111, 61 Av. de l'Observatoire, 75014 Paris, France

⁹ The Niels Bohr Institute, Juliane Maries Vej 30, DK-2100 Copenhagen, Denmark

¹⁰ Nordic Optical Telescope, Apartado 474, ES-38700 Santa Cruz de La Palma, Spain

¹¹ University of Texas at Austin, Department of Astronomy, Austin, TX 78712, USA

¹² Michigan State University, Department of Physics & Astronomy, and JINA: Joint Institute for Nuclear Physics, East Lansing, MI 48824, USA

¹³ INAF - Osservatorio Astronomico di Trieste, via Tiepolo 11, I-34143 Trieste, Italy

Received July 5, 2012; Accepted November 8, 2012.

ABSTRACT

Context. Detailed abundances of the elements produced by r-process nucleosynthesis in various circumstances are our best observational clues to their origin, since the site(s) of r-element production is(are) still not known with certainty. A small fraction of extremely metal-poor (EMP) stars exhibit excesses of heavy neutron-capture elements produced in the r-process, and CS 31082-001 is among the 4 well-known r-process-enhanced EMP stars. Observations with HST/STIS provide abundances for elements observable only from the UV region. The third peak elements were analyzed in a previous paper, and here we present a complete analysis of heavy elements based on the near-UV spectra from HST/STIS and a new VLT/UVES spectrum.

Aims. Here we aim to supplement the optical data with abundances from near-UV spectroscopy of the first and second peak of the r-elements, which are crucial to giving insight into the nucleosynthesis of the elements beyond iron. The UVES spectrum provided additional measurements, thereby improving the previous results.

Methods. The spectra were analyzed with the OSMARCS LTE model atmosphere and with a consistent approach based on the spectrum synthesis code Turbospectrum to derive abundances of heavy elements in CS 31082-001, using updated oscillator strengths from the recent literature. We computed synthetic spectra for all lines of the elements of interest, checking for proper intensities and possible blends. We combined the abundances of heavy elements derived in previous works with the derivation of abundances from all reliable new list of lines, for the first and second peaks of r-elements.

Results. We were able to derive new abundances for 23 n-elements, 6 of them - Ge, Mo, Lu, Ta, W, and Re - were not available in previous works, making this star the most complete r-II object studied, with a total of 37 detections of n-capture elements. We also present the first NLTE+3D lead abundance in this star. The results provide improved constraints on the nature of the r-process.

Key words. Galaxy: Halo - Stars: Abundances - stars: individual: BPS CS 31082-001 - nucleosynthesis

1. Introduction

The origin of the elements beyond the iron peak has been described as the result of two major mechanisms of neutron capture, the s-process and the r-process. The s-process occurs at a slower rate than the half-life of beta decay, while the r-process

Send offprint requests to: C. Siqueira Mello Jr., email: cesar.mello@usp.br).

[★] Based on observations made with the NASA/ESA Hubble Space Telescope (HST) through the Space Telescope Science Institute, operated by the Association of Universities for Research in Astronomy, Inc., under NASA contract NAS5-26555; and with the ESO Very Large Telescope at Paranal Observatory, Chile; Progr. ID 165.N-0276.

occurs at a rapid rate, which is shorter than the beta decay intervention timescale (Burbidge et al. 1957). The difference in the timescale is associated with different neutron fluxes, which are used by the seed nuclei to build heavier nuclei, and as a consequence, completely different sites are needed to allow for these mechanisms to occur. However, the site(s) of r-element production is(are) still not known with certainty (e.g. Wanajo 2006; Kratz et al. 2007; Thielemann et al. 2010).

The popular models involve high-entropy neutrino-driven winds of neutron-rich matter, which build up heavy nuclei near the neutrino sphere of a core-collapse supernova (Woosley et al. 1994; Wanajo 2007, and references therein). Studies of

the Galactic chemical evolution confirm the likelihood of core-collapse supernovae, in particular near their low-mass end (8-10 M_{\odot}), as the dominant source of r-process elements (e.g. Mathews & Cowan 1990; Ishimaru & Wanajo 1999).

However, hydrodynamical simulations with accurate neutrino transport show that neutrino winds are proton-rich (Fischer et al. 2010; Hüpdepohl et al. 2010) or only slightly neutron-rich (Martínez-Pinedo et al. 2012; Roberts 2012; Roberts et al. 2012) and not very neutron-rich as found in some older simulations (Woosley et al. 1994). Since hydrodynamical simulations still encounter difficulties reproducing the astrophysical conditions of the process, the neutrino wind scenario for the origin of the heavy r-process elements is doubtful.

Neutron-rich ejecta from neutron star-neutron star (NS-NS) or black hole-neutron star (BH-NS) binary mergers have been suggested as plausible alternative astrophysical sites of the main r-process (Lattimer et al. 1977; Meyer 1989; Freiburghaus et al. 1999; Surman et al. 2008; Goriely et al. 2011; Wanajo & Janka 2012; Korobkin et al. 2012).

As recently discussed in Peterson (2011), studies of the origin of the lightest trans-Fe elements, from gallium through cadmium ($Z = 31$ to 48), are even more complex. These elements have been attributed in varying degrees to a weak s-process (Clayton 1968; Käppeler et al. 1989), to a so-called light element primary process (LEPP; Travaglio et al. 2004) such as a weak r-process (Wanajo & Ishimaru 2006; Farouqi et al. 2010; Wanajo et al. 2011), and/or to the νp -process (Fröhlich et al. 2006; Pruet et al. 2006; Wanajo 2006; Arcones & Montes 2011) in core-collapse supernovae.

Detailed abundances of the elements produced by r-process nucleosynthesis in various circumstances are our best observational clues to the nature of this mechanism, and a quite good picture can be obtained by considering the products of heavy-element production in the first generation(s) of stars, as recorded in the low-mass stars that survive until today. Actually, neutron-capture elements are present in some of the oldest stars, which are Galactic halo stars extremely metal-poor (EMP), and studies of their abundance are being employed to provide clues to and constraints on the nature of the synthesis and the identities of the stellar generations in the early Galaxy, and also to provide new insight into the astrophysical site(s) for the r-process.

CS 31082-001 is in the group of the 12 EMP r-II¹ giant stars known, and it is one of the most extreme r-element enhanced giants. Actually, together with CS 22892-052 and HE 1523-0901, this star has attracted the most attention, and its abundance patterns have been studied in considerable detail. Recently, Barbuy et al. (2011) did a complete analysis of the third-peak r-process elements and actinides abundances in CS 31082-001 using near UV HST/STIS spectra.

In the present paper, we analyze the first- and second-peak r-elements from near UV lines in the same STIS spectra and a new UVES/VLT spectrum centered at 340 nm. The first peak comprises the elements $38 \leq Z \leq 48$, while the second peak comprises $56 \leq Z \leq 72$, including the lanthanides ($57 \leq Z \leq 71$). These elements can be produced in both the slow and rapid neutron-capture processes, but Truran (1981) argued that in EMP stars these elements are predominantly due to r-processes because intermediate-mass AGB stars had no time to enrich the matter before the formation of the observed EMP stars.

This work is organized as follows. Section 2 describes the observations and data reduction; Sect. 3 summarizes the procedures of abundance determination, as well as the adopted final

abundances for each element; Sect. 4 discusses the results in the context of r-process models; Sect. 5 summarizes our conclusions.

2. Observations

CS 31082-001 was observed with the Space Telescope Imaging Spectrograph (STIS) in the near UV (program ID 9359; PI: R. Cayrel). STIS spectroscopic mode E230M combines an échelle grating with an NUV-MAMA detector to obtain spectra in the wavelength range 1575-3100 Å, at a resolution of $R=30000$. More information can be found in Barbuy et al. (2011).

As a complement to these observations we used the mean of three UVES spectra centered at 340 nm, obtained in 2001 at the VLT on October 20, 21, and 22, in the framework of the ESO Large Program “First Stars”. In the common range of wavelengths ($300\text{nm} < \lambda < 307\text{nm}$), the co-added spectrum has a higher resolution ($R=75000$) than the HST spectrum, and a S/N of about 20 at 300 nm and 100 at 340 nm, and it was not used by Hill et al. (2002). The reduction of these spectra was performed using the UVES context within MIDAS: bias subtraction, fit and subtraction of the interorder background from the object, and flat-field images. The wavelength calibration was performed on Th-Ar lamp frames and used to build a co-added spectrum.

3. Abundance determination

The present abundance determinations are based on the OS-MARCS LTE atmospheric model (Gustafsson et al. 2003, 2008), which use an updated version of the MARCS program (Gustafsson et al. 1975; Plez et al. 1992; Asplund et al. 1997) to build 1D LTE plane-parallel models for cool stars. As done by Hill et al. (2002) and Barbuy et al. (2011), we used a consistent approach based on the spectrum synthesis code Turbospectrum (Alvarez & Plez 1998), which includes a full chemical equilibrium and Van der Waals collisional broadening by H, He, and H₂, following Anstee & O’Mara (1995), Barklem & O’Mara (1997), and Barklem et al. (1998). The code also properly accounts for scattering in the continuum, an important effect in the UV (Cayrel et al. 2004; Barbuy et al. 2011). The stellar parameters are adopted from Hill et al. (2002): $T_{\text{eff}} = 4825 \pm 50$ K, $\log g = 1.5 \pm 0.3$, $[\text{Fe}/\text{H}] = -2.9 \pm 0.1$ (in LTE), and $v_t = 1.8 \pm 0.2$ km s⁻¹. We also adopted the light element abundances determined by Hill et al. (2002), Cayrel et al. (2004), and Spite et al. (2005).

The calculations used the Turbospectrum molecular line lists, described detailedly in Alvarez & Plez (1998), together with the atomic line lists from the VALD2 compilation (Kupka et al. 1999), unless updated oscillator strengths were available in the literature: Cr I from Sobek et al. (2007); Ge I from Bié-mont et al. (1999); La II from Lawler et al. (2001a); Ce II from Palmeri et al. (2000) and Lawler et al. (2009); Nd II from Den Hartog et al. (2003); Sm II from Lawler et al. (2006); Eu I and Eu II from Lawler et al. (2001b) and Den Hartog et al. (2002); Gd II from Den Hartog et al. (2006); Tb II from Lawler et al. (2001c); Dy II from Sneden et al. (2009); Er II from Lawler et al. (2008); Tm I and Tm II from Wickliffe & Lawler (1997) and Sneden et al. (2009); Lu I from Fedchak et al. (2000); Lu II from Quinet et al. (1999); Hf II from Lawler et al. (2007); Ta I from Fivet et al. (2006); W II from Nilsson et al. (2008).

Following the same procedure as in Barbuy et al. (2011), we computed synthetic spectra for all lines of the elements of interest from our line list, with different enhancement factors, in order to identify useful lines. All lines were checked for proper intensities and possible blends, and lines with major and/or uncertain

¹ Following the classification from Beers & Christlieb (2005).

Table 1. LTE abundances in CS 31082-001 as derived from previous works, from the present paper, and our adopted final abundances.

El.	Z	A(X)	A(X)	A(X)	A(X)	A(X)	[X/Fe]
		(1)	(2)	(3)	This Work	adopted	adopted
Ge	32	—	—	—	+0.10	+0.10±0.21	-0.55
Sr	38	+0.72	—	—	—	+0.72±0.10	0.73
Y	39	-0.23	—	—	-0.15	-0.19±0.07	0.53
Zr	40	+0.43	—	—	+0.55	+0.49±0.08	0.84
Nb	41	-0.55	—	—	-0.52	-0.54±0.12	0.97
Mo	42	—	—	—	-0.11	-0.11±0.13	0.90
Ru	44	+0.36	—	—	+0.36	+0.36±0.12	1.45
Rh	45	-0.42	—	—	-0.42	-0.42±0.12	1.39
Pd	46	-0.05	—	—	-0.09	-0.09±0.07	1.18
Ag	47	-0.81	—	—	-0.84	-0.84±0.21	1.15
Ba	56	+0.40	—	—	—	+0.40±0.14	1.16
La	57	-0.60	-0.62	—	—	-0.62±0.05	1.17
Ce	58	-0.31	-0.29	—	-0.31	-0.29±0.05	1.03
Pr	59	-0.86	-0.79	—	—	-0.79±0.05	1.38
Nd	60	-0.13	-0.15	—	-0.21	-0.15±0.05	1.33
Sm	62	-0.51	-0.42	—	-0.42	-0.42±0.05	1.51
Eu	63	-0.76	-0.72	—	-0.75	-0.72±0.05	1.69
Gd	64	-0.27	-0.21	—	-0.29	-0.21±0.05	1.61
Tb	65	-1.26	-1.01	—	-1.00	-1.01±0.05	1.64
Dy	66	-0.21	-0.07	—	-0.12	-0.07±0.05	1.73
Ho	67	—	-0.80	—	—	-0.80±0.06	1.62
Er	68	-0.27	-0.30	—	-0.31	-0.30±0.05	1.67
Tm	69	-1.24	-1.15	—	-1.18	-1.15±0.05	1.64
Yb	70	—	-0.41	—	—	-0.41±0.11	1.66
Lu	71	—	—	—	-1.08	-1.08±0.13	1.73
Hf	72	-0.59	-0.72	—	-0.73	-0.72±0.05	1.33
Ta	73	—	—	—	-1.60	-1.60±0.23	1.47
W	74	—	—	—	-0.90	-0.90±0.24	0.92
Re	75	—	—	—	-0.21	-0.21±0.21	2.45
Os	76	+0.43	—	+0.18	—	+0.18±0.07	1.72
Ir	77	+0.20	—	+0.20	—	+0.20±0.07	1.72
Pt	78	—	—	+0.30	—	+0.30±0.23	1.46
Au	79	—	—	-1.00	—	-1.00±0.34	0.89
Pb	82	—	—	-0.65	—	-0.65±0.19	0.25
Bi	83	—	—	-0.40	—	-0.40±0.33	1.83
Th	90	-0.98	—	—	—	-0.98±0.13	1.84
U	92	-1.92	—	—	—	-1.92±0.17	1.68

References. (1) Hill et al. (2002), (2) Sneden et al. (2009), (3) Barbuy et al. (2011).

blends were rejected. As discussed by Peterson et al. (2001), modeling the UV region is difficult because of the crowding of lines at short wavelengths. Another extreme problem is the number of “unknown” lines (absent from the input line list), resulting in difficulties to match observations and spectral synthesis calculations, making it more difficult to normalize the UV continuum. Recently, Peterson (2011) has reported determinations of the molybdenum abundances in five mildly to extremely metal-poor turnoff stars using near-UV spectra with a “guessed identifications” method of missing lines (for the details on the procedure, see Peterson et al. 2001). In this work we preferred to reject those lines seriously affected by these effects.

3.1. Final abundances

The selected lines and individual abundances are available in Table A.1. The mean abundances $A(X)^2$ for 23 neutron capture elements are given in Table 1 (column 6) and compared to previous measurements (Hill et al. 2002; Sneden et al. 2009). We were able to derive the abundances of six newly studied elements: germanium (Ge, $Z=32$), molybdenum (Mo, $Z=42$), lutetium (Lu, $Z=71$), tantalum (Ta, $Z=73$), tungsten (W, $Z=74$), and rhenium (Re, $Z=75$). The general agreement is discussed in section 3.3. We also investigated the elements in the region between germa-

² We adopt the notation $A(X) = \log \epsilon(X) = \log n(X)/n(H) + 12$, with n = number density of atoms.

Table 2. Solar r - and s -process fractions (Simmerer et al. 2004) and total solar abundances elements. Adopted abundances are marked in boldface. *: Meteoritic abundances.

El.	Z	Fraction			$A(X)_\odot$				
		r	s	(1)	(2)	(3)	(4)	(5)	
Fe	26	—	—	7.67	7.50	7.50	7.45	7.52	—
Ge	32	0.516	0.484	3.41	3.41	3.65	3.58	—	—
Sr	38	0.110	0.890	2.90	2.97	2.87	2.92	—	—
Y	39	0.281	0.719	2.24	2.24	2.21	2.21	—	—
Zr	40	0.191	0.809	2.60	2.60	2.58	2.58	—	—
Nb	41	0.324	0.676	1.42	1.42	1.46	1.42	—	—
Mo	42	0.323	0.677	1.92	1.92	1.88	1.92	—	—
Ru	44	0.610	0.390	1.84	1.84	1.75	1.84	—	—
Rh	45	0.839	0.161	1.12	1.12	0.91	1.12	—	—
Pd	46	0.555	0.445	1.69	1.69	1.57	1.66	—	—
Ag	47	0.788	0.212	1.24*	1.24*	0.94	0.94	—	—
Sn	50	0.225	0.775	2.0	2.0	2.04	2.00	—	—
Ba	56	0.147	0.853	2.13	2.13	2.18	2.18	—	—
La	57	0.246	0.754	1.22	1.17	1.10	1.14	—	—
Ce	58	0.186	0.814	1.55	1.58	1.58	1.61	—	—
Pr	59	0.508	0.492	0.71	0.71	0.72	0.76	—	—
Nd	60	0.421	0.579	1.50	1.50	1.42	1.45	—	—
Sm	62	0.669	0.331	1.00	1.01	0.96	1.00	—	—
Eu	63	0.973	0.027	0.51	0.51	0.52	0.52	0.52	—
Gd	64	0.819	0.181	1.12	1.12	1.07	1.11	—	—
Tb	65	0.933	0.067	0.33*	0.35*	0.30	0.28	—	—
Dy	66	0.879	0.121	1.10	1.14	1.10	1.13	—	—
Ho	67	0.936	0.064	0.26	0.26	0.48	0.51	—	—
Er	68	0.832	0.168	0.93	0.93	0.92	0.96	—	—
Tm	69	0.829	0.171	0.13*	0.15*	0.10	0.14	—	—
Yb	70	0.682	0.318	1.08	1.08	0.84	0.86	—	—
Lu	71	0.796	0.204	0.12*	0.06	0.10	0.12	—	—
Hf	72	0.510	0.490	0.88	0.88	0.85	0.88	0.87	—
Ta	73	0.588	0.412	0.13*	-0.13*	-0.12*	-0.14*	—	—
W	74	0.462	0.538	0.68*	0.69*	0.85	1.11	—	—
Re	75	0.911	0.089	0.27*	0.28*	0.26*	0.28*	—	—
Os	76	0.916	0.084	1.45	1.45	1.40	1.45	1.36	—
Ir	77	0.988	0.012	1.35	1.35	1.38	1.38	—	—
Pt	78	0.949	0.051	1.8	1.8	1.62*	1.74	—	—
Au	79	0.944	0.056	1.01	1.01	0.92	1.01	—	—
Pb	82	0.214	0.786	1.85	1.95	1.75	2.00	—	—
Bi	83	0.647	0.353	0.71*	0.71*	0.65*	0.67*	—	—
Th	90	1.000	0.000	0.12	0.08*	0.02	<0.08	0.08	—
U	92	1.000	0.000	<-0.47	<-0.47	-0.54*	<-0.47	—	—

References. (1): Anders & Grevesse (1989); (2): Grevesse & Sauval (1998); (3): Asplund et al. (2009); (4): Lodders et al. (2009); (5): Caffau et al. (2011).

mium and strontium, as well the elements between the first and the second peaks of the r -process, but no useful line was found.

As noted above, many elements of the first and second peaks of the r -process in these metal-poor stars are observable from the ground, and several authors have presented analyses of them, so for each element, we compared the new abundance with the previous data in order to adopt a final value. The results are shown in the columns 7 and 8 of Table 1.

For comparison, the solar abundances from different authors in the literature (Anders & Grevesse 1989; Grevesse & Sauval 1998; Sneden et al. 2008; Asplund et al. 2009; Lodders et al. 2009; Caffau et al. 2011) are listed in Table 2 for all elements of interest. In this work we adopted the values from Lodders et al. (2009) and Caffau et al. (2011). We also present the Solar System r - and s -process deconvolution of Simmerer et al. (2004), and use the fractions of r -process from the deconvolution of Simmerer et al. (2004) with the adopted solar system abundances.

3.2. Uncertainties on the derived abundances

As discussed by Cayrel et al. (2004), for a given stellar temperature, the ionization equilibrium provides an estimate of the stellar gravity with an internal accuracy of about 0.1 dex in log

g , and the microturbulence velocity v_t can be constrained within 0.2 km s^{-1} , making of the temperature the largest source of uncertainties in the abundance determination. In fact, the authors estimate that the total error on the adopted temperatures is on the order of 100 K, higher than the previous estimation found by Hill et al. (2002).

We estimate the abundance uncertainties arising from each of these three sources independently. The results are shown in the Table 3 (columns 3 to 5), where the models B, C, and D are compared with our nominal model labeled A.

Since the stellar parameters are not independent of each other, the total error budget is not the quadratic sum of the various sources of uncertainties, but it does contain significant covariance terms. The solution was to create a new atmospheric model with a temperature higher by 100 K, thereby determining the corresponding surface gravity by requiring that the Fe derived from Fe I and Fe II lines be identical, and the microturbulent velocity requiring that the abundance derived for individual Fe I lines to be independent of the equivalent width of the line. The model E is the result of this method, with $T_{\text{eff}} = 4925 \text{ K}$, $\log g = 1.8 \text{ dex}$, and $v_t = 1.8 \text{ km s}^{-1}$, and Table 3 (column 6) shows abundance uncertainties arising from stellar parameters.

Observational errors were estimated using the standard deviation of the abundances from the individual lines for each element, and they must take the uncertainties in defining the continuum, fitting the line profiles, and in the oscillator strengths into account. For elements presenting only three useful lines, we conservatively adopted the typical observational error obtained for molybdenum as representative of these cases, and when the number of lines for a given element is only two or less we adopted 0.2 dex, as described in section 3.3.1.

Finally, we examined the adopted resolution for the synthetic spectrum calculation as another possible source of uncertainties. Barbuy et al. (2011) discuss in detail this value ($R=30\,800$) which includes the effect of the instrumental profile, the macro-turbulence and the rotational velocities of the stars. Analyzing the lines again, we checked that a change of 8 % in R induces a variation in the abundances of at most 0.05 dex, which we take into account for all elements in the final error.

3.3. Elements of the first peak

3.3.1. Germanium ($Z=32$)

The Ge I 3039.067 Å line is the main abundance indicator for this element. Using the Biémont et al. (1999) gf -value we were able to determine an abundance of $A(\text{Ge})=0.10\pm 0.21 \text{ dex}$, a first detection of this element in CS 31082-001. Since we only used one line, we checked the influence of the placement of the continuum on the derived abundance, as shown in Fig. 1, and we assumed an observational error of $\sigma=0.2 \text{ dex}$ as a good estimation of this value. We also used this observation uncertainty with other elements which present only two lines or a single one. In fact, since such lines have a better definition of the continuum than the Ge line, we assume this 0.2 dex value as an upper limit, in particular with the UVES spectrum.

Our result of $[\text{Ge}/\text{Fe}]=-0.55$ agrees with those found by Cowan et al. (2002, 2005) in metal-poor galactic halo stars, showing that germanium is strongly depleted compared to the solar abundance ratio, even in r-rich metal-poor stars.

Table 3. Abundance uncertainties linked to stellar parameters.

El.	Δ_{B-A}	Δ_{C-A}	Δ_{D-A}	Δ_{E-A}
A: $T_{\text{eff}} = 4825$, $\log g = 1.5 \text{ dex}$, $v_t = 1.8 \text{ km s}^{-1}$				
B: $T_{\text{eff}} = 4825$, $\log g = 1.4 \text{ dex}$, $v_t = 1.8 \text{ km s}^{-1}$				
C: $T_{\text{eff}} = 4825$, $\log g = 1.5 \text{ dex}$, $v_t = 1.6 \text{ km s}^{-1}$				
D: $T_{\text{eff}} = 4925$, $\log g = 1.5 \text{ dex}$, $v_t = 1.8 \text{ km s}^{-1}$				
E: $T_{\text{eff}} = 4925$, $\log g = 1.8 \text{ dex}$, $v_t = 1.8 \text{ km s}^{-1}$				
[Fe/H]	-0.01	+0.04	+0.06	+0.10
[Ge I/Fe]	+0.01	-0.03	+0.09	+0.05
[Y II/Fe]	-0.01	+0.12	+0.03	+0.05
[Zr II/Fe]	-0.01	+0.06	+0.02	+0.06
[Nb II/Fe]	-0.02	-0.02	+0.03	+0.09
[Mo II/Fe]	-0.02	-0.02	+0.01	+0.07
[Ru I/Fe]	+0.02	-0.03	+0.10	+0.04
[Rh I/Fe]	+0.02	-0.04	+0.09	+0.04
[Pd I/Fe]	+0.02	-0.02	+0.09	+0.04
[Ag I/Fe]	+0.02	-0.03	+0.10	+0.04
[Ce II/Fe]	-0.02	-0.03	+0.03	+0.08
[Nd II/Fe]	-0.02	-0.03	+0.03	+0.08
[Sm II/Fe]	-0.02	-0.02	+0.03	+0.08
[Eu II/Fe]	-0.01	+0.07	+0.03	+0.07
[Gd II/Fe]	-0.02	+0.01	+0.03	+0.07
[Tb II/Fe]	-0.02	-0.02	+0.03	+0.08
[Dy II/Fe]	-0.01	+0.07	+0.03	+0.06
[Er II/Fe]	-0.02	+0.01	+0.02	+0.07
[Tm II/Fe]	-0.02	-0.01	+0.02	+0.07
[Lu II/Fe]	-0.02	-0.03	+0.01	+0.07
[Hf II/Fe]	-0.02	-0.01	+0.03	+0.08
[Ta II/Fe]	-0.03	-0.03	+0.04	+0.11
[W II/Fe]	-0.03	-0.02	+0.05	+0.12
[Re II/Fe]	-0.03	-0.02	-0.01	+0.06

3.3.2. Yttrium ($Z=39$)

Using 13 new Y II lines with other two lines already used in Hill et al. (2002), we are able to determine an abundance of $A(\text{Y})=-0.15\pm 0.07 \text{ dex}$ for this element, in agreement with $A(\text{Y})=-0.23\pm 0.12 \text{ dex}$ found previously. In fact, both of the lines in common between Hill et al. (2002) and the present work show compatible results, leading us to adopt the average $A(\text{Y})=-0.19\pm 0.07 \text{ dex}$ ($[\text{Y}/\text{Fe}]=0.53$) as the final abundance.

Recently, Hansen et al. (2012) analyzed a sample of metal-poor stars, including CS 31082-001. They also adopted MARCS models, but for CS 31082-001, a slightly different set of atmospheric parameters ($T_{\text{eff}}=4925 \text{ K}$, $\log g=1.51 \text{ [cgs]}$, $V_t=1.4$, $[\text{Fe}/\text{H}]=-2.81$). For the spectrum synthesis they adopted MOOG (Snedden 1973, version 2009 including treatment of scattering). The difference between their $[\text{X}/\text{Fe}]$ results and our adopted values is in general lower than 0.1, but for yttrium they found $[\text{Y}/\text{Fe}]=0.82$, which is 0.29 higher than our adopted value.

We decided to check this comparison in a homogeneous way, using the code Turbospectrum to determine the Y abundance in CS 31082-001 using the lines from Hansen et al. (2012) with our set of atmospheric parameters as well as with their values.

We find $[\text{Y}/\text{Fe}]=0.47$ with our original atmospheric parameters, while the atmospheric parameters of Hansen et al. (2012) give the relative abundance $[\text{Y}/\text{Fe}]=0.71$, and the difference 0.24 is very close to the previous one. However, we found a stronger correlation between the individual abundances and the equivalent widths with the atmospheric parameters adopted by Hansen et al. (2012), suggesting that their microturbulence velocity is underestimated. In fact, when only changing the v_t in their set

of atmospheric parameters to our microturbulence velocity we found $[Y/Fe]=0.47$, in agreement with our adopted value, confirming the problem with their v_t . Yttrium is particularly sensitive to this effect because several Y lines are relatively strong.

3.3.3. Zirconium ($Z=40$)

More than 25 Zr II profiles were checked in STIS spectrum but we decided to keep the 12 best lines, and together with more 46 UVES new useful lines, we find a final abundance $A(Zr)=+0.55\pm 0.08$ dex for the zirconium, in agreement with the value $A(Zr)=+0.43\pm 0.14$ dex from Hill et al. (2002). Figure 2 shows two fits of lines used in this work. The line Zr II 2758.792 Å gives an abundance of $A(Zr)=-0.07$ dex, despite a good fit, suggesting there is a problem with the gf-value of the transition and leading us to exclude this line from the average. The same applies to Zr II 3556.585 Å line, which gives $A(Zr)=0.00$ dex. We are using a larger set of lines than in previous work, and the abundances of the transitions used by Hill et al. (2002) can be considered as a subset of our data. Finally, the line Zr II 3030.915 Å was used with both spectra STIS and UVES and we found compatible results. All this evidence suggests that the average $A(Zr)=+0.49\pm 0.08$ dex ($[Zr/Fe]=0.84$) is the best choice for the adopted final abundance.

3.3.4. Niobium ($Z=41$)

While only one line was used in Hill et al. (2002) to derive an abundance of $A(Nb)=-0.55\pm 0.20$ dex, we were able to find nine useful Nb II lines from an initial set with more than 70 lines, giving an average abundance of $A(Nb)=-0.52\pm 0.11$ dex, in good agreement with the previous value. In Fig. 3 we show an example of fit to a Nb II line.

It was possible to again use both of the spectra with the same line Nb II 3028.433 Å, and we found agreement between the results. It makes the average a good indicator for the abundance of niobium, and we adopted $A(Nb)=-0.54\pm 0.12$ dex ($[Nb/Fe]=0.97$) as the final value.

3.3.5. Molybdenum ($Z=42$)

After checking almost 50 Mo lines, the spectra presented three Mo II useful lines, giving $A(Mo)=-0.11\pm 0.13$ dex ($[Mo/Fe]=0.90$). Despite all the previous analysis done, this is the first published value of $A(Mo)$ in this star. The lines 2660.576 Å, 2871.507 Å, and 2930.485 Å used here are shown in Figs. 4, 5, and 6.

3.3.6. Ruthenium ($Z=44$)

The VALD atomic data for many transitions of Ru I give equivalent widths that are too strong, as discussed by Barbuy et al. (2011), and new laboratory oscillator strengths have not been presented in the recent literature. However, we tried to use one Ru I line to determine a new UV abundance from STIS, and we found $A(Ru)=0.65$ dex, higher than the previous result $A(Ru)=0.36\pm 0.17$ dex from Hill et al. (2002), confirming the impossibility of using the region of the STIS spectra for this element.

We calculated the abundance again using the three lines observed in our new UVES spectrum, and also used by Hill et al. (2002) and we found $A(Ru)=0.36\pm 0.12$ dex ($[Ru/Fe]=1.45$), in very good agreement with the previous work.

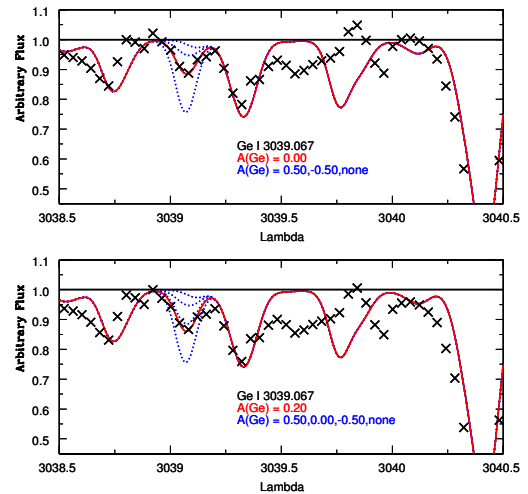


Fig. 1. Fits of the observed Ge I 3039.067 Å line in CS 31082-001 for two different placements of the continuum. Crosses: observations. Dotted lines: synthetic spectra computed for the abundances indicated in the figure. Solid line: synthetic spectrum computed with the best abundance, also indicated in the figure.

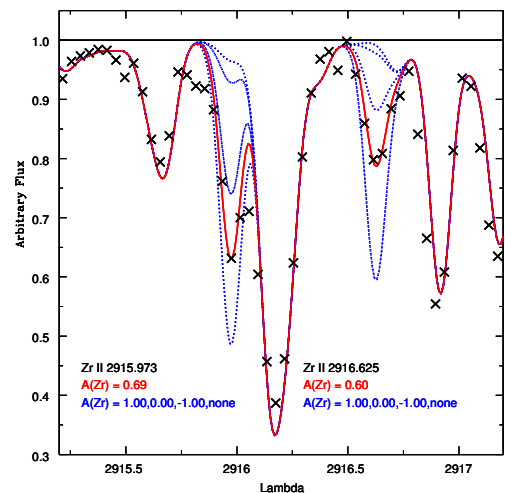


Fig. 2. Fits of the observed Zr II 2915.973 Å and Zr II 2916.625 Å lines in CS 31082-001. Symbols as in Fig. 1.

3.3.7. Rhodium ($Z=45$)

Using three good Rh I lines, we were able to determine $A(Rh)=-0.42\pm 0.12$ dex ($[Rh/Fe]=1.39$) for the abundance of this element. Our new result is in complete agreement with $A(Rh)=-0.42\pm 0.16$ dex from Hill et al. (2002) and this value was adopted as the final abundance.

3.3.8. Palladium ($Z=46$)

Adding the line Pd I 3516.944 Å to the original set of transitions from Hill et al. (2002), the new UVES spectra give $A(Pd)=-0.09\pm 0.07$ dex, in good agreement with $A(Pd)=-0.05\pm 0.18$ dex from the previous work. Here we have adopted our new result $[Pd/Fe]=1.18$ as the final abundance.

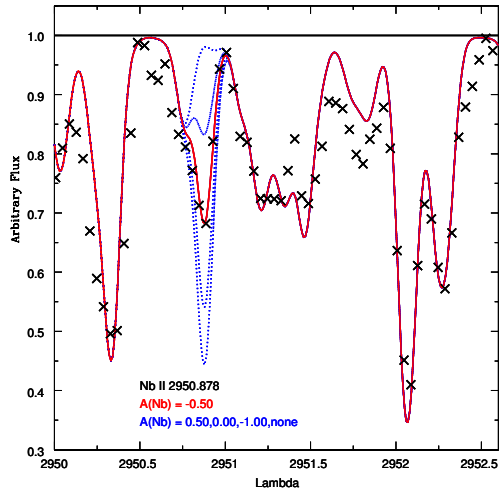


Fig. 3. Fit of the observed Nb II 2950.878 Å line in CS 31082-001. Symbols as in Fig. 1.

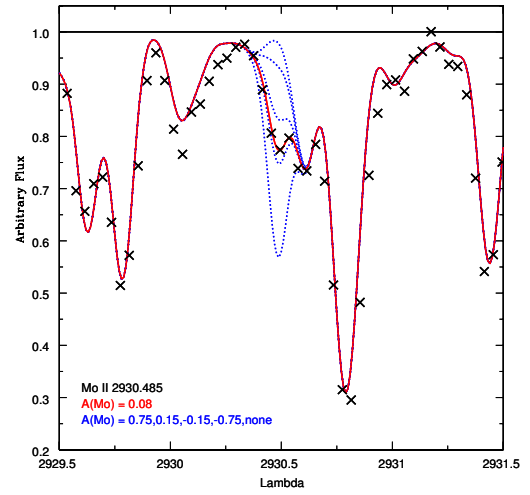


Fig. 6. Fit of the observed Mo II 2930.485 Å line in CS 31082-001. Symbols as in Fig. 1.

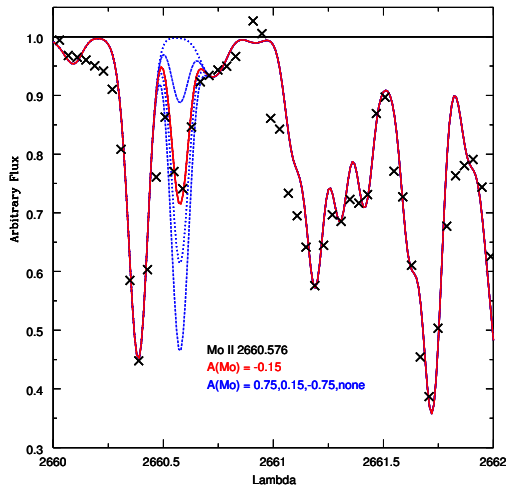


Fig. 4. Fit of the observed Mo II 2660.576 Å line in CS 31082-001. Symbols as in Fig. 1.

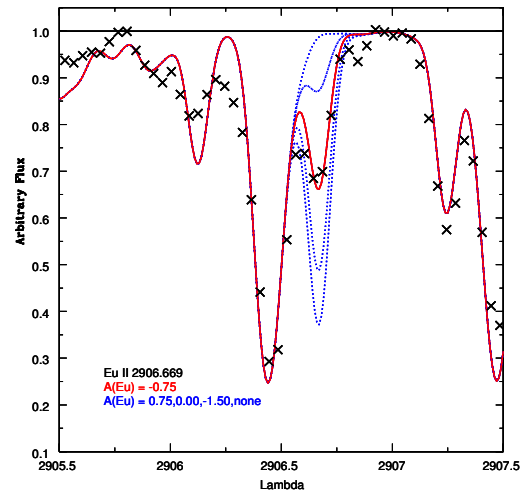


Fig. 7. Fit of the observed Eu II 2906.669 Å line in CS 31082-001. Symbols as in Fig. 1.

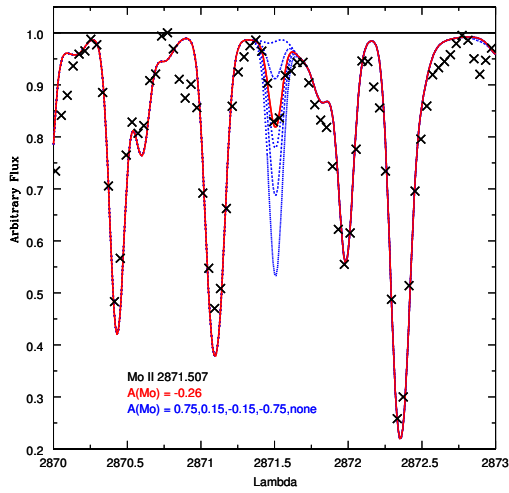


Fig. 5. Fit of the observed Mo II 2871.507 Å line in CS 31082-001. Symbols as in Fig. 1.

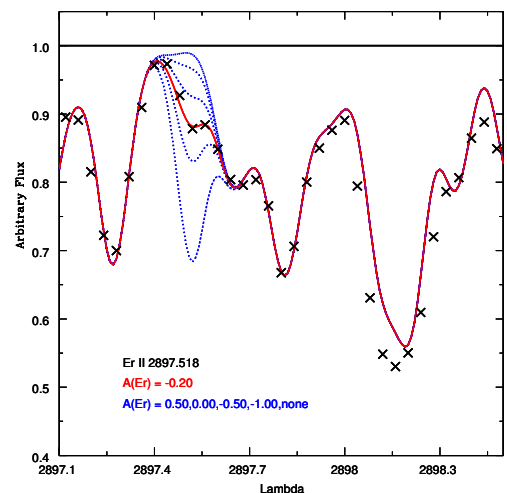


Fig. 8. Fit of the observed Er II 2897.518 Å line in CS 31082-001. Symbols as in Fig. 1.

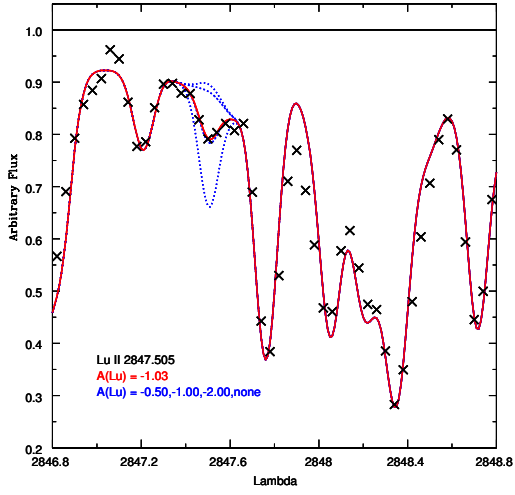


Fig. 9. Fit of the observed Lu II 2847.505 Å line in CS 31082-001. Symbols as in Fig. 1.

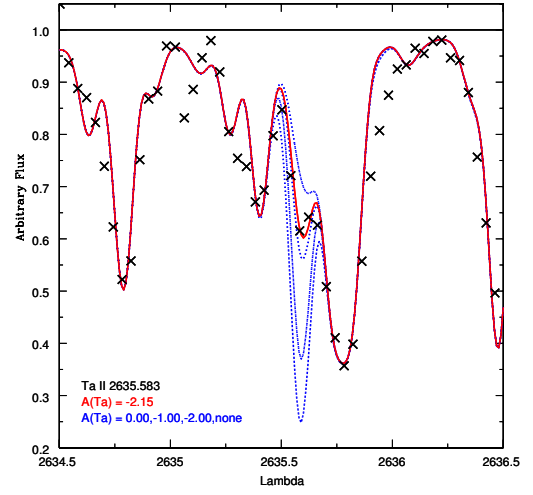


Fig. 12. Fit of the observed Ta II 2635.583 Å line in CS 31082-001. Symbols as in Fig. 1.

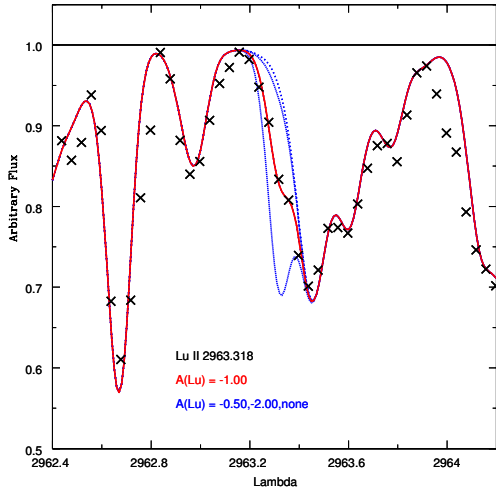


Fig. 10. Fit of the observed Lu II 2963.318 Å line in CS 31082-001. Symbols as in Fig. 1.

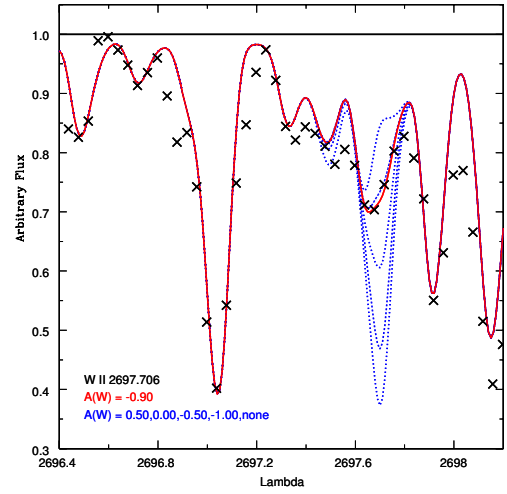


Fig. 13. Fit of the observed W II 2697.706 Å line in CS 31082-001. Symbols as in Fig. 1.

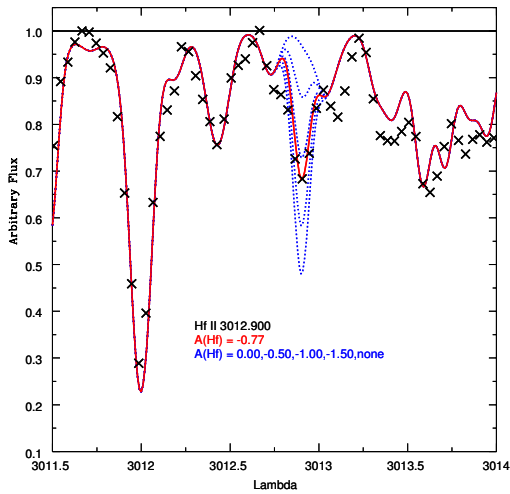


Fig. 11. Fit of the observed Hf II 3012.900 Å line in CS 31082-001. Symbols as in Fig. 1.

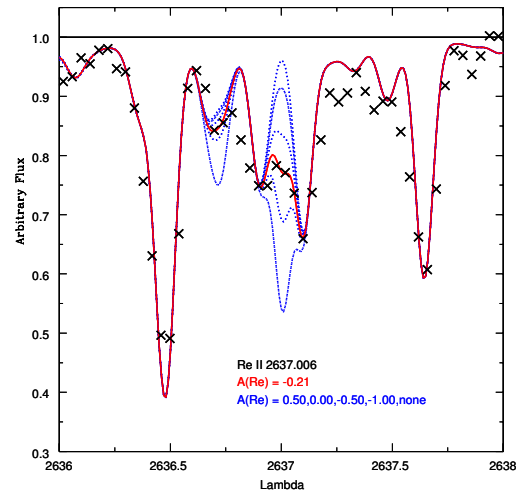


Fig. 14. Fit of the observed Re II 2637.006 Å line in CS 31082-001. Symbols as in Fig. 1.

3.3.9. Silver (Z=47)

For this element, only the Ag I lines 3280.679 Å and 3382.889 Å were useful with the UVES spectrum, the same ones as used by Hill et al. (2002). Our new analysis gives $A(\text{Ag})=-0.84\pm 0.21$ dex ($[\text{Ag}/\text{Fe}]=1.15$) as the final abundance, in agreement with the previous result $A(\text{Ag})=-0.81\pm 0.24$ dex. The lower error found in the present work is probably due to the better quality of the new UVES spectra in the bluer region.

3.4. Elements of the second peak

3.4.1. Barium (Z=56)

This is another element studied by Hansen et al. (2012) in CS 31082-001 with a big difference when compared with previous results. They found $[\text{Ba}/\text{Fe}]=1.43$, which is 0.27 higher than our adopted value from Hill et al. (2002). While the abundance in this last work was derived from six Ba II lines, Hansen et al. (2012) used only two of them, Ba II 4554.03 Å and Ba II 5853.67 Å, leading us to check these results again.

In addition to the comments made in the case of yttrium, we also adopted the same reference as for the hyperfine structure of barium (McWilliam 1998). The final abundance was calculated with the weighting method suggested by the authors to allow us a genuine comparison (for details, see Hansen et al. 2012). We found $[\text{Ba}/\text{Fe}]=1.04$ with our original atmospheric parameters, while the set from Hansen et al. (2012) gave the relative abundance $[\text{Ba}/\text{Fe}]=1.30$. The difference between the results is 0.26, very close to the previous difference. Since the barium lines are strong, we explain this difference as effect of the microturbulence velocity, and we decided to keep the result from Hill et al. (2002) as the final abundance. Considerations about the NLTE corrections on this result can be found in section 3.5.

3.4.2. Cerium (Z=58)

By using ten new lines of Ce II we were able to determine the abundance $A(\text{Ce})=-0.31\pm 0.10$ dex, in very good agreement with the value from Hill et al. (2002). However, Sneden et al. (2009) determined a more precise abundance using 38 transitions for this element, leading us to adopt their result $A(\text{Ce})=-0.29\pm 0.05$ dex ($[\text{Ce}/\text{Fe}]=1.03$) as the final abundance.

3.4.3. Neodymium (Z=60)

We derived an abundance $A(\text{Nd})=-0.21\pm 0.10$ dex from the 18 useful Nd II lines in the region covered by the new UVES spectra, in agreement with $A(\text{Nd})=-0.13\pm 0.13$ dex found by Hill et al. (2002) and with $A(\text{Nd})=-0.15\pm 0.05$ dex by Sneden et al. (2009), despite the lower absolute value. In fact, even using only the subset of lines with improved atomic data we found $A(\text{Nd})=-0.24\pm 0.10$ dex, quite similar to the complete set. Other authors use sets of lines covering the entire optical region, and we adopted the result from Sneden et al. (2009) $[\text{Nd}/\text{Fe}]=1.33$ as the final abundance, since they have used the most complete line list for this element.

3.4.4. Samarium (Z=62)

This element presents 23 useful lines in the region studied, and we found the abundance $A(\text{Sm})=-0.42\pm 0.09$ dex from the set of data, in complete agreement with $A(\text{Sm})=-0.42\pm 0.05$ dex ($[\text{Sm}/\text{Fe}]=1.51$) from Sneden et al. (2009). We decided to keep

this last result as the adopted abundance since the number of lines used is considerably higher, making the error smaller.

3.4.5. Europium (Z=63)

After checking more than 20 profiles, we derived the abundance $A(\text{Eu})=-0.75\pm 0.22$ dex from the best Eu II 2906.669 Å, in agreement with $A(\text{Eu})=-0.72\pm 0.05$ dex from Sneden et al. (2009). Fig. 7 shows our fit to this line. We finally adopted the value from Sneden et al. (2009) as the more reliable result ($[\text{Eu}/\text{Fe}]=1.69$) given the higher number of lines used.

3.4.6. Gadolinium (Z=64)

This element shows several available lines in this region, and we derived its abundance using 32 Gd II lines. We found $A(\text{Gd})=-0.29\pm 0.09$ dex, in agreement with $A(\text{Gd})=-0.21\pm 0.05$ from Sneden et al. (2009).

In this work we are using the same references as Sneden et al. (2009) for new atomic data, but not all the transitions have been updated by Den Hartog et al. (2006), so we adopted the value from Sneden et al. (2009) as more reliable ($[\text{Gd}/\text{Fe}]=1.61$).

3.4.7. Terbium (Z=65)

This is the most problematic element with respect to compatibility between previous abundance results. Hill et al. (2002) found $A(\text{Tb})=-1.26\pm 0.12$ dex with $\sigma=0.07$ from seven optical lines using the UVES spectra, while Sneden et al. (2009) found $A(\text{Tb})=-1.01\pm 0.05$ dex with $\sigma=0.04$ from nine lines using updated oscillator strengths from Lawler et al. (2001c). In this work we were able to use three Tb II lines to derive the abundance $A(\text{Tb})=-1.00\pm 0.14$ dex. For the line 2934.802 Å no new gf-value is available so it was excluded from the average, despite a good fit.

Our new result confirms the lower abundance found by Sneden et al. (2009), and we decided to keep $[\text{Tb}/\text{Fe}]=1.64$ as the more reliable abundance since the authors used a bigger set of lines.

3.4.8. Dysprosium (Z=66)

From 26 profiles in the region studied, we determined the abundance $A(\text{Dy})=-0.16\pm 0.09$ dex. By selecting only those lines with new atomic data, the abundance found is $A(\text{Dy})=-0.12\pm 0.09$ dex, in agreement with $A(\text{Dy})=-0.07\pm 0.05$ dex from Sneden et al. (2009). We finally readopted the value resulting from the largest set of lines $[\text{Dy}/\text{Fe}]=1.73$ from Sneden et al. (2009) as the final abundance.

3.4.9. Erbium (Z=68)

After checking several Er lines, we were able to derive a new abundance $A(\text{Er})=-0.31\pm 0.09$ dex from 17 good lines of Er II. Fig. 8 shows an example of fit to an Er II line. Our result agrees with $A(\text{Er})=-0.27\pm 0.15$ dex found by Hill et al. (2002) and with $A(\text{Er})=-0.30\pm 0.05$ dex found by Sneden et al. (2009), which used the same reference for atomic data. However, the last authors derived their result from 19 erbium lines, with $\sigma=0.04$, which combined with our higher uncertainty, leads us to keep the value $[\text{Er}/\text{Fe}]=1.67$ found by Sneden et al. (2009) as the most reliable.

3.4.10. Thulium (Z=69)

From several Tm lines, we were able to use the nine best lines to derive an abundance $A(\text{Tm}) = -1.18 \pm 0.10$ dex. Our result agrees with $A(\text{Tm}) = -1.24 \pm 0.13$ dex by Hill et al. (2002) and $A(\text{Tm}) = -1.15 \pm 0.05$ dex by Sneden et al. (2009).

3.4.11. Lutetium (Z=71)

Another new element derived in CS 31082-001, the adopted abundance is $A(\text{Lu}) = -1.08 \pm 0.13$ dex ($[\text{Lu}/\text{Fe}] = 1.73$), obtained from the mean of the results derived from the three best Lu II lines (see Figs. 9 and 10) from our set of data.

3.4.12. Hafnium (Z=72)

After checking more than 60 lines in the region studied, we derived a hafnium abundance $A(\text{Hf}) = -0.73 \pm 0.11$ dex from five lines that were not affected by unidentified lines or other problems. Figure 11 shows an example of fit to an Hf II line. Our result is in good agreement with $A(\text{Hf}) = -0.72 \pm 0.05$ dex ($[\text{Hf}/\text{Fe}] = 1.33$) from Sneden et al. (2009), which used new atomic data from Lawler et al. (2007). We decided to keep the last result as the most reliable abundance.

3.4.13. Tantalum (Z=73)

As discussed in Barbuy et al. (2011), this is another element that presents lines that are too strong for many transitions from the VALD database, and also an element that has not been analyzed in this star. We found new oscillator strengths for five Ta I lines in Fivet et al. (2006), but all of them were discarded for typical problems of UV region (as the definition of the continuum). However, we tried to use three other Ta II lines present in the spectrum.

Ta II 2685.190 Å gives $A(\text{Ta}) = -2.80$ dex, but the synthetic profile of the line is really strong and probably its oscillator strength value is not correct. On the other hand, Ta II 2832.702 Å gives us an abundance $A(\text{Ta}) = -1.05$ dex with a good fit, despite the line being weak. Another abundance indicator is the Ta II 2635.583 Å line, shown in Fig. 12, which yields $A(\text{Ta}) = -2.15$ dex. The final tantalum abundance is the average of the last two lines, $A(\text{Ta}) = -1.60 \pm 0.23$ dex ($[\text{Ta}/\text{Fe}] = 1.47$).

3.4.14. Tungsten (Z=74)

From our set of W II lines, most of them have new atomic data presented in Nilsson et al. (2008). We derived the abundance $A(\text{W}) = -0.90 \pm 0.24$ dex ($[\text{W}/\text{Fe}] = 0.92$) using our best line W II 2697.706 Å, shown in Fig. 13, also another first determination in this star.

3.4.15. Rhenium (Z=75)

For the heaviest element analyzed in this work and also a new one for this star, the abundance $A(\text{Re}) = -0.21 \pm 0.21$ dex ($[\text{Re}/\text{Fe}] = 2.45$) was derived from our two best lines Re I 2930.613 Å and Re II 2637.006 Å (see Fig. 14). Together with tungsten, rhenium abundance is extremely important for studying the transition region between the second and the third peaks of the r-process.

3.5. NLTE and tridimensional corrections

Andrievsky et al. (2009, 2011) reanalyzed the sample of the EMP stars previously studied in the framework of the ESO Large program “First Stars”, including CS 31082-001, determining in particular the abundance of Sr and Ba based on NLTE computations. For Sr the NLTE abundance is 0.2 dex lower than the LTE value found in Hill et al. (2002) ($[\text{Sr}/\text{Fe}]_{\text{NLTE}} = 0.53$), while a stronger correction to the Ba abundance was found, and the NLTE value is $A(\text{Ba}) = 0.00$ dex ($[\text{Ba}/\text{Fe}]_{\text{NLTE}} = 0.76$).

Recently, Mashonkina et al. (2012) have considered the ultraviolet overionization to calculate the NLTE abundance of Pb in cool stars for the Pb I line 4057 Å. In the case of CS 31082-001 the corrected value is $A(\text{Pb}) = +0.01$ ($[\text{Pb}/\text{Fe}]_{\text{NLTE}} = 0.94$), substantially higher than the previous LTE abundances $A(\text{Pb}) = -0.55$ from Plez et al. (2004) and $A(\text{Pb}) = -0.65$ from Barbuy et al. (2011). For completeness, we also present the NLTE abundance for europium calculated by Mashonkina et al. (2012), 0.06 dex higher ($[\text{Eu}/\text{Fe}]_{\text{NLTE}} = 1.75$) than the best LTE value $A(\text{Eu}) = -0.72$ dex from Sneden et al. (2009).

For the other heavy elements NLTE corrections are not available. It would be particularly interesting to check the NLTE effects on the Ge abundances, since the main abundance indicator for this element is a transition from the non ionized state.

It is well known that NLTE calculations relative to LTE have effects on the abundances that are counterbalanced by taking 3D modeling into account, therefore both effects should be computed at the same time. In fact, since the lead abundance is an important calibration point for zero-age r-process abundance distribution models (Schatz et al. 2002; Wanajo 2007), and the NLTE correction found in the literature is high enough to have implications for the discussion of r-process models for the heaviest n-capture elements in this star, we calculated the 3D correction for the abundance of this element.

For computing of the 3D correction we used a hydrodynamical model computed with the code CO5BOLD (Freytag et al. 2002, 2012) with parameters 5020/2.5/-3/0. The model has a resolution of $160 \times 160 \times 200$, and its dimension is $573215 \times 573214 \times 245362$ km³. Twenty representative snapshots have been selected, covering 156 h in time. For the opacity, based on the MARCS stellar atmosphere package (Gustafsson et al. 2008), the absorption coefficients were averaged in six bins. The plane parallel 1D_{LHD} model was used as reference model, computed with the LHD code that shares the micro-physics and opacity with the CO5BOLD code.

The 3D correction is defined as $A(3D) - A(1D_{\text{LHD}})$ (for details, see Caffau et al. 2011). The line formation computations were done with Linfor3D³. Compared with the 1D LTE value, the 3D effect presents a correction of $\Delta A(\text{Pb}) = -0.21$ dex, which together with the NLTE correction, gives a new lead abundance of $A(\text{Pb}) = -0.20$ dex ($[\text{Pb}/\text{Fe}]_{\text{NLTE}} = 0.73$). As discussed by Spite et al. (2012), weaker lines form in deeper layers, where the granulation velocities and intensity contrast are higher, which is a possible explanation for this significant correction in the lead abundance.

It is important to note that our correction is not a full 3D NLTE computation, which has only been performed for Li I and O I so far. But while these complete models seem to be important in the Li case (Asplund et al. 2003; Barklem et al. 2003; Cayrel et al. 2007; Sbordone et al. 2010), the NLTE corrections for O I are quite similar in the 3D and 1D cases, at least with the solar parameters (Asplund et al. 2004).

³ http://www.aip.de/~mst/Linfor3D/linfor_3D_manual.pdf

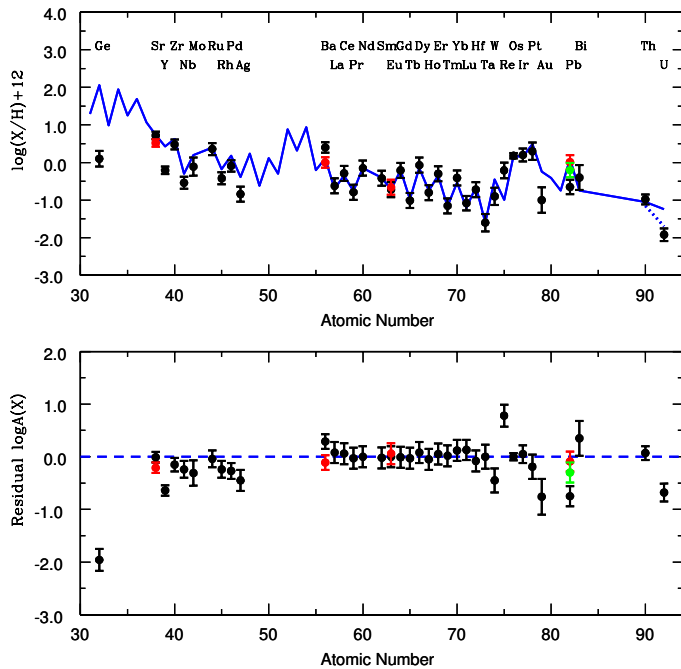


Fig. 15. Solar r-process abundance values. Top: deconvolution from Simmerer et al. (2004) scaled to Eu (solid line) compared with the new complete observed abundances in CS 31082-001 (black dots and respective error bars). Radioactive element (Th and U) abundances are corrected for radioactive decay since the formation of the solar system. The dotted line shows the abundances observed today for these two species. Bottom: Abundance residuals. NLTE abundances for some elements (red dots and respective error bars) are compared with the LTE results. For Pb, the green symbol represents the NLTE+3D corrected value.

4. Discussion

4.1. Comparison with the solar system r-process pattern

The abundances in CS 31082-001 as determined from previous works (Hill et al. 2002; Sneden et al. 2009) and from the present analysis are compared with each other in Table 1. A comparison of the observed abundance pattern with the scaled solar system r-process abundances using the deconvolution from Simmerer et al. (2004) is shown in Fig. 15, together with the residual values. The figure includes the results from Barbuy et al. (2011) for the third-peak r-process elements. For the radioactive elements U and Th, the abundance corrected for radioactive decay since the formation of the solar system, and the abundances observed today are shown. In addition, the available NLTE abundances for some elements (red dots and respective error bars) are compared with the LTE results, and in the case of lead we also present the new NLTE+3D corrected abundance as the green symbol.

Fig. 15 shows the NLTE corrected abundances compared with the LTE result and with the solar system r-process abundances, from which it is possible to see that the NLTE corrections from Andrievsky et al. (2011) make the Sr abundance more similar to the trends of the other elements from the first peak. One can also see from Fig. 15 that the NLTE Ba abundance from Andrievsky et al. (2009) is in good agreement with the Solar System r-process pattern. Finally, the comparison shows that the new NLTE+3D lead abundance is in better agreement but still lower than the solar system r-process value.

As discussed in some detail in the last section, there is clear compatibility of the observational results for each element. Furthermore, Fig. 15 shows that the n-capture element distribution in the star matches a scaled solar r-process pattern very well, from Ba ($Z=56$) through the third r-process peak. This well-known result in the context of metal-poor stars enriched in r-process elements had led some authors to argue that this extremely close agreement is evidence of the robust nature of the r-process, operating in much the same manner over the lifetime of the Galaxy. Our new abundances for lutetium and tantalum follow this trend, but while the tungsten value seems to be under-solar, the rhenium is overabundant. The disagreement can originate in a break down of the universality for $Z = 74-75$, from our spectrum and/or the atomic data, but another possible error source is the solar system r-process deconvolution (Goriely 1999).

Sneden et al. (2008) present an abundance comparison in their Fig. 11 with extensive elemental data for six r-process-rich stars, including CS 31082-001, showing exactly the consistency between the abundances of the heavier stable n-capture elements and the solar system r-process abundance distribution. This group of stars has been identified as standard templates to characterize the r-process nucleosynthesis pattern. At the same time, the comparison shows that the match between the stellar r-process abundances and the scaled solar system r-process pattern does not extend to the lighter heavy elements, and Fig. 15 shows this well known result for the specific case of CS 31082-001 with the new abundance determination of molybdenum and germanium. Recently, Roederer et al. (2010a) and Cowan et al. (2011) have proposed that, similarly to the need of having several mechanisms operating, in order to explain the origin of the lightest trans-Fe elements, a simple linear combination of the scaled solar system s-process and r-process is an inadequate description of some of the heavy n-capture elements, when a precise deconvolution is desired. On the other hand, the standard method of computing r-process residuals by solar deconvolution is still adequate for assessing the relative dominance of the s- or r-process in a general sense.

In addition, as discussed in Barbuy et al. (2011), we also see disagreements between observation and theory among the heaviest elements from the third r-process peak and actinides; notably, the high ages derived from the U/Os, U/Ir, and U/Pt ratios in the radioactive chronometry context would indicate that the nuclear data and/or astrophysical modeling of elements production are in need of improvement. On the other hand, that a strong actinide boost is observed in CS 31082-001, but not in other r-II stars like HE 1523-0901, suggests that the production of the heaviest elements in the r-process site(s) may be more complex than supposed so far.

4.2. Comparison with r-process models

Figure 16 compares the predictions of the hot and cold models by Wanajo (2007) with the observed abundances in CS 31082-001, including the new elements derived in this work, while Fig. 17 shows the corresponding residuals. The abundances obtained from these models of nucleosynthesis calculations are based on supernovae neutrino wind models with updated nuclear input data (based on the HFB-9 model of Goriely et al. 2005). These data update the older calculations by Wanajo et al. (2002), who adopted a cold r-process that proceeds with competing (n, γ) and β -decays, but without (γ, n) decays when the temperature drops down to 1.0×10^8 K. This differs from the traditional (hot) r-

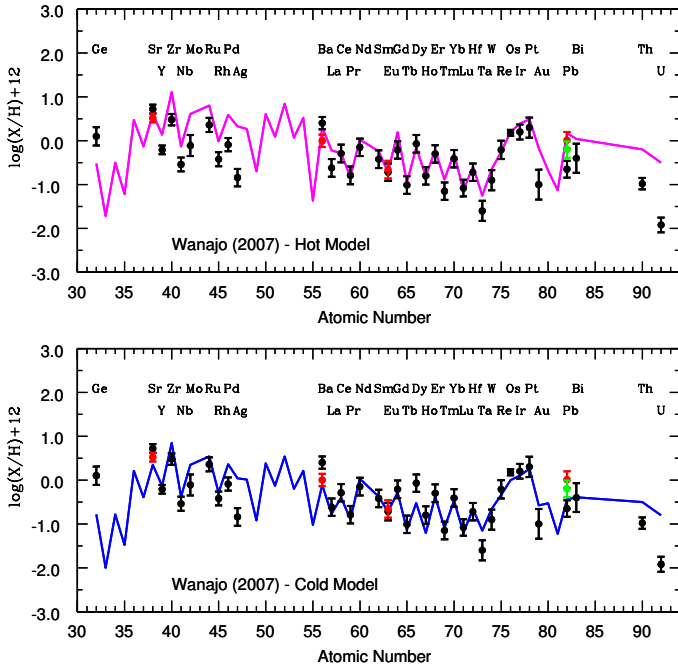


Fig. 16. Predicted abundance patterns for the hot (upper) and cold (lower) models by Wanajo (2007) (solid lines), compared with the new complete observed abundances in CS 31082-001. Symbols as in Fig. 15.

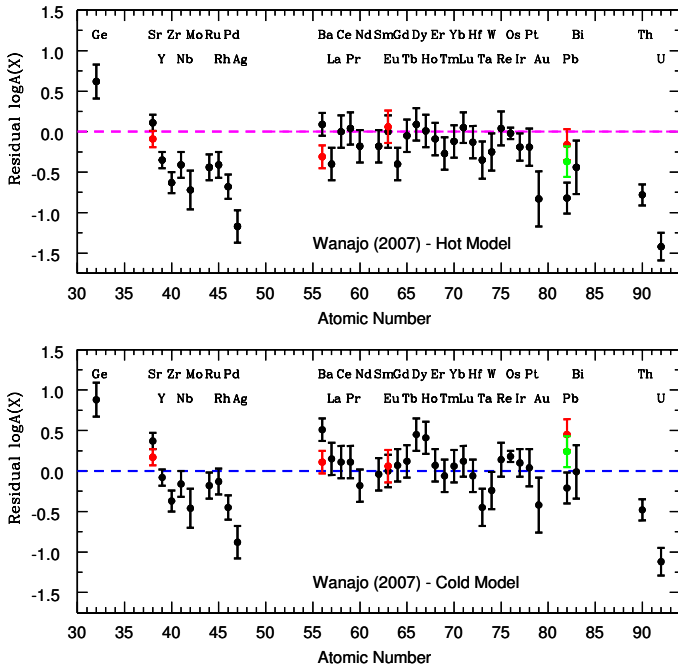


Fig. 17. Abundance residuals of elements in CS 31082-001 from the two Wanajo (2007) model predictions. Symbols as in Fig. 15.

process at a temperature of 1.0×10^9 K, where the (n, γ) - (γ, n) equilibrium remains a good approximation during r-processing.

The hot model fits many of the second-peak elements well, but fails for the first-peak elements and the heaviest third-peak elements. The cold model gives an overall better fit, except for

Ba, Dy, Ho, and Os. This might suggest that the abundance pattern results from nucleosynthetic processes in several different physical conditions. It is also worth noting that both the hot and cold models fit our new Lu, W, and Re abundances very well (for two of which poor agreement with the solar r-pattern can be seen in Fig. 15), despite the failure to fit the Ta abundance. We note that it is the first time that abundances of elements from the region between the second and third peaks are given for an EMP star. An important difference between the models is the behavior of the abundance pattern for the heaviest elements of the third peak. While the traditional “hot model” from Wanajo et al. (2002) produces abundances of gold, lead, and bismuth that are substantially higher than the observed values, the cold model seems to be better for describing this region, as discussed in Barbuy et al. (2011). Albeit more subtly, the new NLTE+3D Pb abundance leads us to the same conclusion. It would be interesting to check these corrections with the other elements in this region, but NLTE corrections for gold and bismuth are not available in the literature, any more than the 3D corrections.

Recently, Farouqi et al. (2010) have investigated the termination point of charged-particle freezeout, and they define a maximum entropy for a given expansion velocity and electron abundance (Y_e), beyond which the seed production of heavy elements fails owing to the very low matter density. They also investigated an r-process subsequent to the charged-particle freeze-out, analyzing the impact of nuclear properties from different theoretical mass models on the final abundances. They find it is possible to coproduce the light p-, s-, and r-process isotopes between Zn ($Z = 30$) and Ru ($Z = 44$) at Y_e in the range 0.450-0.498 and low entropies of $S < 100$ -150 k_B (Boltzmann constant) per nucleon (see also similar discussion in Hoffman et al. 1996; Wanajo 2006). They also show that for Y_e slightly below 0.50, only the mass region below the mass number $A=130$ peak can be formed, and the classical “main” r-process region up to the full third peak requires somewhat more neutron-rich winds. Figure 18 shows the results from Farouqi et al. (2010) with $Y_e=0.498$ and $Y_e=0.482$, compared with the observed abundances in CS 31082-001. The calculations were performed with a selected constant expansion velocity of $V_{exp} = 7500$ km s $^{-1}$, and for each Y_e the superposition of the entropies spans from $S = 5$ k_B /nucleon to the maximum entropy $S_{final}(Y_e) \sim 300$ k_B /nucleon. One can see that the whole mass region from Sr up to Th can be fitted by using different parameters, in agreement with the need for more than one site for the r-process and/or different conditions into the same environment. This study can be seen as a generalization of the hot and cold models from Wanajo (2007), since the parametrization should reach the entire range of possibilities.

4.3. Origin of germanium

Another important approach to understanding the origin of the elements is to check the evolution of their abundances as a function of the metallicity, from a sample of star. However, for some elements, the number of stars with determined abundances is still reduced by the difficulty of detection. That is the case of germanium and molybdenum. Cowan et al. (2005) used a sample of ten metal-poor Galactic halo stars with measures of Ge to analyze the behavior of this light element compared to the principal r-process patterns, represented by the Eu abundance. The sample includes the r-poor star HD 122563. We reproduce the original comparison including CS 31082-001 in the sample with our new Ge abundance. The result is shown in the Fig. 19, and one can see that our star is the most metal-poor object in the sample (Fig. 19 top), and the most enriched with r-process el-

ements (Fig. 19 bottom). The Ge abundance is correlated with metallicity, but seems to be uncorrelated with the r-process elements. The authors also discuss that while n-capture processes are important for Ge production in solar system material, these abundance comparisons immediately suggest a different origin for this element early in the history of the Galaxy.

It is important to note that the neutrino-driven wind always predicts $\text{Ge}/\text{Sr} < 1$, because the high entropy ($S > 30 k_B/\text{nucleon}$) leads to charged-particle freezeout from nuclear statistical equilibrium (NSE) and makes the abundance peak at $N = 50$ nuclei ^{88}Sr , ^{89}Y , and ^{90}Zr (Woosley & Hoffman 1992; Meyer et al. 1998; Wanajo & Ishimaru 2006). In contrast, the early convective ejecta from O-Ne-Mg (electron-capture) supernova predict $\text{Ge}/\text{Sr} \sim 1$, because its low entropy ($S \sim 10 k_B/\text{nucleon}$) with mild neutron-richness (Y_e down to 0.4) leads to form the abundance peak at $A = 70\text{-}80$ ($N < 50$) including Ge in NSE (Hartmann et al. 1985; Wanajo et al. 2011). In Fig. 20 we compare the relative abundances $[\text{Ge}/\text{Sr}]$ with $[\text{Sr}/\text{Eu}]$ for the same sample used in Fig. 19, and one can find a marginal correlation between the Ge enhancement and the weakness of r-processing. The bottom panel in Fig. 20 still compares the abundance of Ge relative to the level of the heavy r-elements in the star, represented by the Eu abundance, as a function of the enhancement in r-process elements. We find a clear anticorrelation between the r-process richness and the Ge enhancement. In fact, our Fig. 18 shows that the low Ge abundance in our r-rich star CS 31082-001 is described better by the neutrino wind models, while the high Ge abundance in the r-poor star HD 122563 is explained well by the electron-capture supernova model (see Fig. 5 in Wanajo et al. 2011). This indicates that Ge serves as a key element in constraining the astrophysical conditions for r-process nucleosynthesis.

It is worth noting that the region between the iron peak and the first peak of the r-process is historically thought to be the beginning of the r-process, and Ge is at the end of the Fe peak. In fact, the noncorrelation between the Ge abundance and the general level of heavy r-elements (Fig. 19, bottom panel), leads us not to discard the possibility of an iron peak (or NSE) origin to Ge. Using a sample of metal-poor stars from Cowan et al. (2005), François et al. (2007), Roederer et al. (2010b), Peterson (2011), and Hansen et al. (2012), we calculated the correlation between $[\text{X}/\text{Fe}]$ with respect to $[\text{Eu}/\text{Fe}]$, where X represents the elements available from the iron peak to the heavy r-elements. Figure 21 shows our results, and represents the average behavior in each group of elements, and in the case of the iron peak the value was calculated without the result for germanium. One can see that the behavior of the germanium is not clear enough to allow us to decide about its origin, and we stress that it is necessary to collect more observational data and perform an NLTE analysis of this element to permit a strong conclusion.

5. Conclusions

For the first time, we have determined abundances of molybdenum and germanium in CS 31082-001, using an STIS spectrum. In fact, there is a lack of results for the stellar abundances of these elements for EMP stars compared to other elements from the first peak, so our new abundance determinations are particularly valuable, and should be seen as part of a big project, from several authors, trying to solve this observational gap as an attempt to understand the origin of the lightest trans-Fe elements.

Following the idea of completing the abundance analysis of this star, we were also able to derive abundances for lutetium

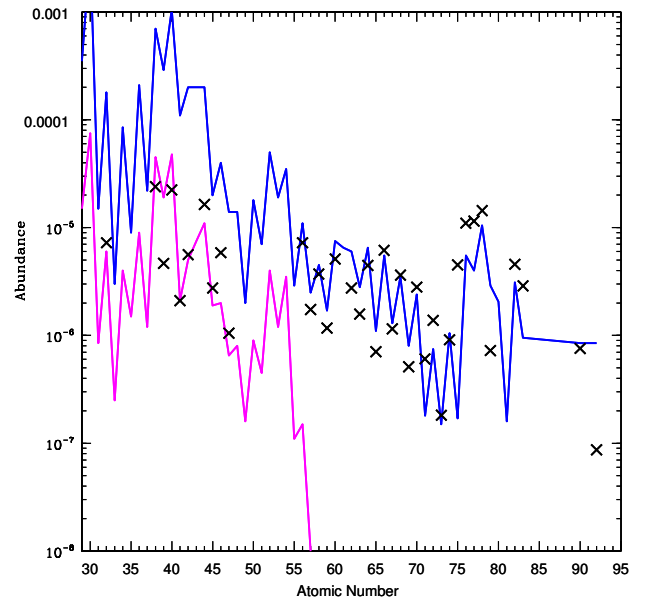


Fig. 18. Comparison of the new complete observed abundances in CS 31082-001 (crosses) with yields from Farouqi et al. (2010), using Y_e of 0.498 (magenta solid line) and 0.482 (blue solid line). For each Y_e the superposition of the entropies spans from $S = 5 k_B/\text{nucleon}$ to the maximum entropy $S_{final}(Y_e) \sim 300 k_B/\text{nucleon}$.

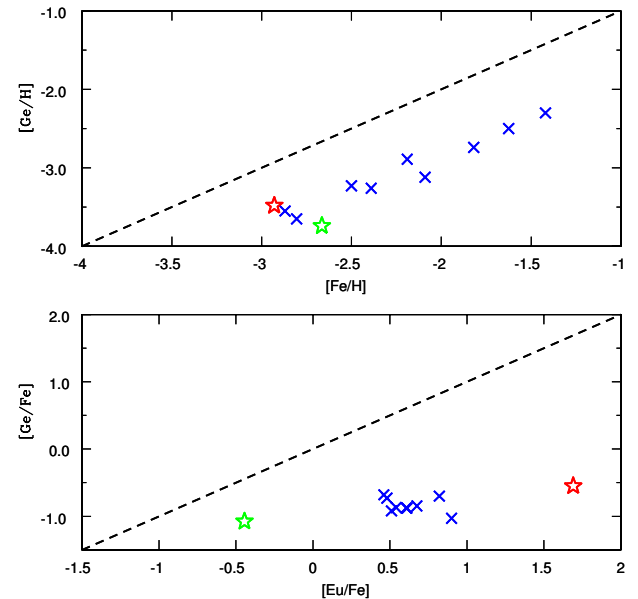


Fig. 19. Relative abundances $[\text{Ge}/\text{H}]$ displayed as a function of $[\text{Fe}/\text{H}]$ metallicity (top) and correlation between the abundance ratios $[\text{Ge}/\text{Fe}]$ and $[\text{Eu}/\text{Fe}]$ (bottom). The blue symbols represent the original data from Cowan et al. (2005) and our new abundances for CS 31082-001 is marked as the red star. The r-poor HD 122563 is marked as the green star. The dashed line indicates the solar abundance ratio of these elements.

and tantalum, other newly determined abundances, which agrees with the solar system r-process abundance, confirming the compatibility between the r-process in EMP stars and the solar system patterns, from Ba through the third r-process peak, which also confirms universal behavior of the process in this range of

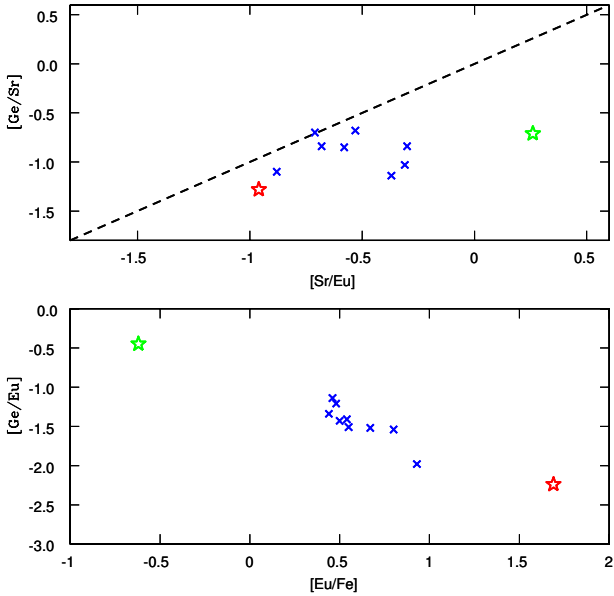


Fig. 20. Relative abundances $[\text{Ge}/\text{Sr}]$ displayed as a function of $[\text{Sr}/\text{Eu}]$ (top) and correlation between the abundance ratios $[\text{Ge}/\text{Eu}]$ and $[\text{Eu}/\text{Fe}]$ (bottom). Symbols as in Fig. 19.

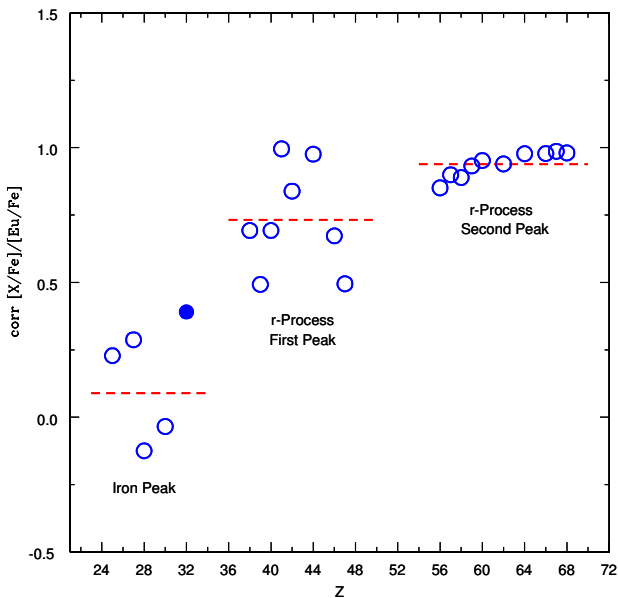


Fig. 21. Correlation between $[\text{X}/\text{Fe}]$ with respect to $[\text{Eu}/\text{Fe}]$ using a sample of metal-poor stars (see text). The germanium is represented as the filled circle. The dashed lines represent the average behavior in each group of elements.

elements. On the other hand, this compatibility does not extend to the lighter heavy elements or to the heaviest elements from the actinides region.

Furthermore, the STIS/HST spectra of CS 31082-001 permitted us to derive the first abundance determination of W and Re in an EMP star, two extremely important elements for studying the transition region between the second and the third peaks of the r-process. Actually, together with the previous abundances, our new results make the star the most complete r-II ob-

ject ever studied, and a major template for studies of r-process models, with a total of 37 detections of n-capture elements, supplanting the previous winner BD+17°3248.

The abundances of the second peak of CS 31082-001 are reasonably well represented by those of the cold model by Wanajo (2007), but not the abundances of the first peak. As in some cases an additional production of the first peak elements by other processes could be invoked. More elegantly, the model of Farouqi with different electron abundances Y_e can explain the first (including Ge) and second peaks. We also present the first NLTE+3D lead abundance in this star, which together with the other heavy elements from the third peak, lead us to underline that supernovae neutrino wind models with lower temperature satisfactorily describes the formation of the elements in this region. In general, the comparisons between calculations and observations do in fact argue for a combination of processes to reproduce the full range of observed stellar abundances.

Acknowledgements. CS and BB acknowledge grants from CAPES, CNPq and FAPESP. MS, VH, BP, RC, FS, PB and PF acknowledge the support of the CNRS (PNCG and PNPS). JA and BN acknowledge partial financial support from the Carlsberg Foundation and the Danish Natural Science Research Council. T.C.B. acknowledges partial funding of this work from grants PHY 02-16783 and PHY 08-22648: Physics Frontier Center/Joint Institute for Nuclear Astrophysics (JINA), awarded by the U.S. National Science Foundation.

References

- Alvarez, R., Plez, B. 1998, *A&A*, 330, 1109
 Anders, E., Grevesse, N. 1989, *Geochim. Cosmochim. Acta*, 53, 197
 Andrievsky, S. M., Spite, M., Korotin, S. A. et al. 2009, *A&A*, 494, 1083
 Andrievsky, S. M., Spite, F., Korotin, S. A. et al. 2011, *A&A*, 530, A105
 Anstee, S. D. & O'Mara, B. J. 1995, *MNRAS*, 276, 859
 Arcones, A. & Montes, F. 2011, *ApJ*, 731, 5
 Asplund, M., Gustafsson, B., Kiselman, D. et al. 1997, *A&A*, 318, 521
 Asplund, M., Carlsson, M., Botnen, A. V. 2003, *A&A*, 399, 31
 Asplund, M., Grevesse, N., Sauval, A. J. et al. 2004, *A&A*, 417, 751
 Asplund, M., Grevesse, N., Sauval, A. J. et al. 2009, *ARA&A*, 47, 481
 Barbuy, B., Spite, M., Hill, V. et al. 2011, *A&A*, 534, 60
 Barklem, P. S. & O'Mara, B. J. 1997, *MNRAS*, 290, 102
 Barklem, P. S., O'Mara, B. J., Ross, J. E. 1998, *MNRAS*, 296, 1057
 Barklem, P. S., Belyaev, A. K., Asplund, M. 2003, *A&A*, 409, 1
 Beers, T. C. & Christlieb, N. 2005, *ARA&A*, 43, 531
 Biémont, E., Grevesse, N., Hannaford, P. et al. 1981, *ApJ*, 248, 867
 Biémont, E., Lynga, C., Li, Z. S. et al. 1999, *MNRAS*, 303, 721
 Burbidge, E. M., Burbidge, G. R., Fowler, W. A. et al. 1957, *Reviews of Modern Physics*, 29, 547
 Caffau, E., Ludwig, H.-G., Steffen, M. et al. 2011, *Solar Phys.*, 268, 255
 Cayrel, R., Depagne, E., Spite, M. et al. 2004, *A&A*, 416, 1117
 Cayrel, R., Steffen, M., Chand, H. et al. 2007, *A&A*, 473, 37
 Clayton, D. D. 1968, *Principles of Stellar Evolution and Nucleosynthesis* (New York: McGraw-Hill)
 Cowan, J. J., Sneden, C., Burles, S. et al. 2002, *ApJ*, 572, 861
 Cowan, J. J., Sneden, C., Beers, T. C. et al. 2005, *ApJ*, 627, 238
 Cowan, J. J., Roederer, I. U., Sneden, C. et al. 2011, *RR Lyrae Stars, Metal-Poor Stars, and the Galaxy*, arXiv 1106.1109
 Den Hartog, E. A., Wickliffe, M. E., Lawler, J. E. 2002, *ApJ*, 141, 255
 Den Hartog, E. A., Lawler, J. E., Sneden, C. et al. 2003, *ApJ*, 148, 543
 Den Hartog, E. A., Lawler, J. E., Sneden, C. et al. 2006, *ApJ*, 167, 292
 Farouqi, K., Kratz, K.-L., Pfeiffer, B. et al. 2010, *ApJ*, 712, 1359
 Fedchak, J. A., Den Hartog, E. A., Lawler, J. E. et al. 2000, *ApJ*, 542, 1109
 Fischer, T., Whitehouse, S. C., Mezzacappa, A. et al. 2010, *A&A*, 517, 80
 Fivet, V., Palmeri, P., Quinet, P. et al. 2006, *EPJD*, 37, 29
 François, P., Depagne, E., Hill, V. et al. 2007, *A&A*, 476, 935
 Freiburghaus, C., Rosswog, S., Thielemann, F.-K. 1999, *ApJ*, 525, L121
 Freytag, B., Steffen, M., Dorch, B. 2002, *Astronomische Nachrichten*, 323, 213
 Freytag, B., Steffen, M., Ludwig, H.-G. et al. 2012, *Journal of Computational Physics*, 231, 919
 Fröhlich, C., Martínez-Pinedo, G., Liebendörfer, M. et al. 2006, *Phys. Rev. Lett.*, 96, 142502
 Goriely, S. 1999, *A&A*, 342, 881
 Goriely, S., Samyn, M., Pearson, J. M. et al. 2005, *Nucl. Phys. A*, 750, 425
 Goriely, S., Bauswein, A., Janka, H.-T. 2011, *ApJ*, 738, L32
 Grevesse, N. & Sauval, J. 1998, *SSRv*, 85, 161

- Gustafsson, B., Bell, R. A., Eriksson, K. et al. 1975, *A&A*, 42, 407
- Gustafsson, B., Edvardsson, B., Eriksson, K. et al 2003 in *Stellar Atmosphere Modeling Werner ASP Conf. Series*, 288, 331.
- Gustafsson, B., Edvardsson, B., Eriksson, K. et al. 2008, *A&A*, 486, 951
- Hannaford, P., Lowe, R. M., Grevesse, N. et al. 1982, *ApJ*, 261, 736
- Hansen, C. J., Primas, F., Hartman, H. et al. 2012, arXiv:1205.4744
- Hartmann, D., Woosley, S. E., El Eid, M. F. 1985, *ApJ*, 297, 837
- Hill, V., Plez, B., Cayrel, R. et al. 2002, *A&A* 387, 560
- Hoffman, R. D., Woosley, S. E., Fuller, G. M. et al. 1996, *ApJ*, 460, 478
- Hüdepohl, L., Müller, B., Janka, H.-T. et al. 2010, *Phys. Rev. Lett.*, 104, 251101
- Ishimaru, Y. & Wanajo, S. 1999, *ApJ*, 511, 33
- Käppeler, F., Beer, H., Wisshak, K. 1989, *Rep. Prog. Phys.*, 52, 945
- Korobkin, O., Rosswog, S., Arcones, A et al. 2012, *MNRAS*, 426, 1940
- Kratz, K.-L., Farouqi, K., Pfeiffer, B. et al. 2007, *ApJ*, 662, 39
- Kupka, F., Piskunov, N., Ryabchikova, T. A. et al. 1999, *A&AS*, 138, 119
- Lattimer, J. M., Mackie, F., Ravenhall, D. G. et al. 1977, *ApJ*, 213, 225
- Lawler, J. E., Bonvallet, G., Sneden, C. 2001a, *ApJ*, 556, 452
- Lawler, J. E., Wickliffe, M. E.; Den Hartog, E. A. et al. 2001b, *ApJ*, 563, 1075
- Lawler, J. E., Wickliffe, M. E., Cowley, C. R. et al. 2001c, *ApJ*, 137, 341
- Lawler, J. E., Den Hartog, E. A., Sneden, C. et al. 2006, *ApJ*, 162, 227
- Lawler, J. E., Den Hartog, E. A., Labby, Z. E. et al. 2007, *ApJ*, 169, 120
- Lawler, J. E., Sneden, C., Cowan, J. J. et al. 2008, *ApJ*, 178, 71
- Lawler, J. E., Sneden, C., Cowan, J. J. et al. 2009, *ApJ*, 182, 51
- Ljung, G., Nilsson, H., Asplund, M. et al. 2006, *A&A*, 456, 1181
- Lodders, K., Palme, H., Gail, H.-P. 2009, *Landolt-Börnstein - Group VI Astronomy and Astrophysics Numerical Data and Functional Relationships in Science and Technology Volume 4B: Solar System*. Edited by J.E. Trümper, 4.4., 44
- Martínez-Pinedo, G., Fischer, T., Lohs, A. et al. 2012, arXiv1205.2793
- Mashonkina, L., Ryabtsev, A., Frebel, A. 2012, *A&A*, 540, A98
- Mathews, G. J. & Cowan, J. J. 1990, *Nature*, 345, 491
- McWilliam, A. 1998, *AJ*, 115, 1640
- Meyer, B. S. 1989, *ApJ*, 343, 254
- Meyer, B. S., McLaughlin, G. C., Fuller, G. M. 1998, *Physical Review C*, 58, 3696
- Nilsson, H., Engström, L., Lundberg, H. et al. 2008, *EPJD*, 49, 13
- Palmeri, P., Quinet, P., Wyart, J.-F. et al. 2000, *Physica Scripta*, 61, 323
- Peterson, R. C., Dorman, B., Rood, R. T. 2001, *ApJ*, 559, 372
- Peterson, R. C. 2011, *ApJ*, 742, 21
- Plez, B., Brett, J. M., Nordlund, A. 1992, *A&A*, 256, 551
- Plez, B., Hill, V., Cayrel, R. et al. 2004 *A&A* 428 L9
- Pruet, J., Hoffman, R. D., Woosley, S. E. et al. 2006, *ApJ*, 644, 1028
- Quinet, P., Palmeri, P., Biémont, E. et al. 1999, *MNRAS*, 307, 934
- Roberts, L. F. 2012, *ApJ*, 755, 126
- Roberts, L. F., Reddy, S., Shen, G. 2012, arXiv:1205.4066
- Roederer, I. U., Sneden, C., Lawler, J. E. et al. 2010a, *ApJ*, 714, L123
- Roederer, I. U., Cowan, J. J., Karakas, A. I. et al. 2010b, *ApJ*, 724, 975
- Sbordone, L., Bonifacio, P., Caffau, E. et al. 2010, *A&A*, 522, 26
- Schatz, H., Toenjes, R., Pfeiffer, B. et al. 2002, *ApJ*, 579, 638
- Sikström, C. M., Pihlemark, H., Nilsson, H. et al. 2001, *Journal of Physics B Atomic Molecular Physics*, 34, 477
- Simmerer, J., Sneden, C., Cowan, J. J. et al. 2004, *ApJ*, 617, 1091
- Sneden, C. A. 1973, PhD thesis, The University of Texas at Austin
- Sneden, C., Cowan, J. J., Gallino, R. 2008, *ARA&A*, 46, 241
- Sneden, C., Lawler, J. E., Cowan, J. J. et al. 2009, *ApJ*, 182, 80
- Sobeck, J. S., Lawler, J. E., Sneden, C. 2007, *ApJ*, 667, 1267
- Spite, M., Cayrel, R., Plez, B. et al. 2005, *A&A*, 430, 655
- Spite, M., Andrievsky, S. M., Spite, F. et al. 2012, *A&A*, 541, 143
- Surman, R., McLaughlin, G. C., Ruffert, M. et al. 2008, *ApJ*, 679, L117
- Thielemann, F.-K., Hirschi, R., Liebendörfer, M. et al. 2010, *Lect. Not. Phys.*, 812, 153
- Travaglio, C., Gallino, R., Arnone, E. et al. 2004, *ApJ*, 601, 864
- Truran, J. W. 1981, *A&A*, 97, 391
- Wanajo, S., Itoh, N., Ishimaru, Y. et al. 2002, *ApJ*, 577, 853
- Wanajo, S. 2006, *ApJ*, 647, 1323
- Wanajo, S. & Ishimaru, I. 2006, *Nucl. Phys. A*, 777, 676
- Wanajo, S. 2007, *ApJ*, 666, L77
- Wanajo, S., Janka, H.-T., Müller, B. 2011, *ApJ*, 726, 15
- Wanajo, S. & Janka, H.-T. 2012, *ApJ*, 746, 180
- Wickliffe, M. E., Salih, S., Lawler, J. E. 1994, *J. Quant. Spec. Radiat. Transf.*, 51, 545
- Wickliffe, M. E. & Lawler, J. E. 1997, *Journal of the Optical Society of America B*, 14, 737
- Woosley, S. E. & Hoffman, R. D. 1992, *ApJ*, 395, 202
- Woosley, S. E., Wilson, J. R., Mathews, G. J. et al. 1994, *ApJ*, 433, 229
- Zhiguo, Z., Li, Z. S., Lundberg, H. et al. 2000, *Journal of Physics B Atomic Molecular Physics*, 33, 521

Appendix A: Line list and atomic data

Table A.1 presents the lines of neutron-capture elements that were used to derive abundances. The wavelengths, excitation potentials, and oscillator strengths are listed, together with references.

Table A.1. Available spectral lines and abundances **obtained in CS 31082-001 using the spectra from HST/STIS and VLT/UVES.**

$\lambda(\text{\AA})$	χ_{ex} (eV)	log gf	A(X) _{STIS}	A(X) _{UVES}	Ref.
Ge I (Z=32)					
3039.067	0.883	-0.040	0.10	—	1
Y II (Z=39)					
3200.272	0.130	-0.430	—	-0.08	2
3203.322	0.104	-0.370	—	-0.07	2
3216.682	0.130	-0.020	—	-0.27	2
3242.280	0.180	0.210	—	-0.10	2
3448.808	0.409	-1.440	—	-0.15	2
3549.005	0.130	-0.280	—	-0.12	2
3584.518	0.104	-0.410	—	-0.13	2
3600.741	0.180	0.280	—	-0.20	2
3601.919	0.104	-0.180	—	-0.18	2
3611.044	0.130	0.110	—	-0.23	2
3628.705	0.130	-0.710	—	-0.13	2
3633.122	0.000	-0.100	—	-0.25	2
3710.294	0.180	0.460	—	-0.11	2
3774.331	0.130	0.210	—	-0.14	2
3788.694	0.104	-0.070	—	-0.13	2
Zr II (Z=40)					
2699.593	0.039	-1.170	0.73	—	3
2732.711	0.095	-0.490	0.72	—	3
2758.792	0.000	-0.560	-0.07	—	3
2818.738	0.959	0.020	0.65	—	4
2915.973	0.466	-0.500	0.69	—	3
2916.625	0.359	-1.110	0.60	—	3
2952.236	0.164	-1.250	0.65	—	4
2962.673	0.359	-0.570	0.65	—	3
3019.832	0.039	-1.130	0.80	—	4
3028.045	0.972	0.020	0.45	—	4
3030.915	0.000	-1.040	0.66	0.60	4
3054.837	1.011	0.180	0.35	—	4
3061.334	0.095	-1.380	0.35	—	4
3095.073	0.039	-0.960	—	0.50	4
3125.926	0.000	-0.883	—	0.69	4
3129.763	0.039	-0.650	—	0.63	4
3133.489	0.959	-0.200	—	0.58	4
3138.683	0.095	-0.460	—	0.57	4
3231.692	0.039	-0.590	—	0.70	4
3241.042	0.039	-0.504	—	0.39	4
3272.221	0.000	-0.700	—	0.70	4
3279.266	0.095	-0.230	—	0.60	4
3284.703	0.000	-0.480	—	0.65	4
3305.153	0.039	-0.690	—	0.68	4
3314.488	0.713	-0.686	—	0.50	4
3334.607	0.559	-0.797	—	0.65	4
3338.414	0.959	-0.578	—	0.40	4
3340.574	0.164	-0.461	—	0.43	4
3356.088	0.095	-0.513	—	0.59	4
3357.264	0.000	-0.736	—	0.70	4
3391.982	0.164	0.463	—	0.70	4
3393.122	0.039	-0.700	—	0.60	4
3402.868	1.532	-0.330	—	0.55	4
3403.673	0.999	-0.576	—	0.45	4
3419.128	0.164	-1.574	—	0.50	4
3424.813	0.039	-1.305	—	0.62	4
3430.514	0.466	-0.164	—	0.54	4
3457.548	0.559	-0.530	—	0.68	4
3479.029	0.527	-0.690	—	0.58	5
3479.383	0.713	0.170	—	0.20	5
3499.560	0.409	-0.810	—	0.44	5

Table A.1. continued.

$\lambda(\text{\AA})$	χ_{ex} (eV)	log gf	A(X) _{STIS}	A(X) _{UVES}	Ref.
3505.682	0.164	-0.360	—	0.60	5
3506.048	1.236	-0.860	—	0.43	4
3520.869	0.559	-1.089	—	0.20	4
3525.803	0.359	-0.653	—	0.25	4
3536.935	0.359	-1.306	—	0.35	4
3551.939	0.095	-0.310	—	0.65	5
3556.585	0.466	0.140	—	0.00	4
3573.055	0.319	-1.041	—	0.63	4
3578.211	1.208	-0.607	—	0.52	4
3588.300	0.409	-1.130	—	0.60	5
3607.373	1.236	-0.640	—	0.35	5
3611.889	1.743	0.450	—	0.25	4
3613.102	0.039	-0.465	—	0.67	4
3614.765	0.359	-0.252	—	0.54	4
3630.004	0.359	-1.110	—	0.52	5
3636.436	0.466	-1.035	—	0.52	4
3674.696	0.319	-0.446	—	0.30	4
3714.794	0.527	-0.930	—	0.72	5
3766.795	0.409	-0.812	—	0.67	4
Nb II (Z=41)					
2876.957	0.439	-0.490	-0.62	—	4
2908.237	0.292	-0.340	-0.62	—	4
2910.581	0.376	-0.190	-0.70	—	4
2911.738	0.326	-0.270	-0.62	—	4
2950.878	0.514	0.210	-0.50	—	4
2994.718	0.514	-0.250	-0.15	—	4
3028.433	0.439	-0.410	-0.38	-0.27	4
3191.093	0.514	-0.260	—	-0.55	4
3215.591	0.439	-0.190	—	-0.58	4
Mo II (Z=42)					
2660.576	1.492	-0.136	-0.15	—	6
2871.507	1.540	0.056	-0.26	—	6
2930.485	1.492	-0.228	0.08	—	6
Ru I (Z=44)					
2874.988	0.000	-0.240	0.65	—	7
3436.736	0.148	0.015	—	0.45	7
3498.942	0.000	0.310	—	0.27	7
3728.025	0.000	0.270	—	0.35	7
Rh I (Z=45)					
3396.819	0.000	0.050	—	-0.45	4
3434.885	0.000	0.450	—	-0.41	4
3700.907	0.190	-0.100	—	-0.40	4
Pd I (Z=46)					
3242.700	0.814	-0.070	—	-0.10	4
3404.579	0.814	0.320	—	-0.18	4
3516.944	0.962	-0.240	—	-0.07	4
3634.690	0.814	0.090	—	-0.02	4
Ag I (Z=47)					
3280.679	0.000	-0.050	—	-1.03	4
3382.889	0.000	-0.377	—	-0.65	4
Ce II (Z=58)					
3263.885	0.459	-0.390	—	-0.40	4
3426.205	0.122	-0.660	—	-0.38	8
3507.941	0.175	-0.960	—	-0.27	8
3520.520	0.175	-0.910	—	-0.32	8
3534.045	0.521	-0.140	—	-0.30	8
3539.079	0.320	-0.270	—	-0.29	8
3577.456	0.470	0.140	—	-0.30	8
3659.225	0.175	-0.670	—	-0.38	8
3709.929	0.122	-0.260	—	-0.20	8
3781.616	0.529	-0.260	—	-0.22	8

Table A.1. continued.

$\lambda(\text{\AA})$	χ_{ex} (eV)	log gf	A(X) _{STIS}	A(X) _{UVES}	Ref.
Nd II (Z=60)					
3285.085	0.000	-1.050	—	-0.08	4
3300.143	0.000	-1.036	—	-0.30	4
3325.889	0.064	-1.174	—	-0.20	4
3334.465	0.182	-0.930	—	-0.22	9
3555.764	0.321	-0.950	—	-0.30	9
3560.718	0.471	-0.500	—	-0.38	9
3598.021	0.064	-1.020	—	-0.22	9
3609.780	0.000	-0.800	—	-0.25	9
3730.577	0.380	-0.611	—	-0.15	4
3738.055	0.559	-0.040	—	-0.21	9
3741.424	0.064	-0.680	—	-0.15	9
3763.472	0.205	-0.430	—	-0.20	9
3779.462	0.182	-0.560	—	-0.26	9
3780.382	0.471	-0.350	—	-0.28	9
3784.245	0.380	0.150	—	-0.13	9
3795.454	0.205	-0.650	—	-0.21	9
3803.471	0.205	-0.390	—	-0.20	9
3808.767	0.064	-0.650	—	-0.12	9
Sm II (Z=62)					
3218.596	0.185	-0.640	—	-0.53	10
3244.686	0.185	-1.330	—	-0.45	10
3253.403	0.104	-0.770	—	-0.55	10
3304.517	0.000	-1.190	—	-0.45	4
3307.027	0.659	-0.301	—	-0.15	4
3321.189	0.378	-0.362	—	-0.43	4
3384.654	0.378	-0.741	—	-0.32	4
3568.271	0.485	0.290	—	-0.35	10
3583.372	0.185	-1.110	—	-0.27	10
3604.281	0.485	-0.030	—	-0.38	10
3609.492	0.277	0.160	—	-0.45	10
3621.210	0.104	-0.510	—	-0.46	10
3627.004	0.277	-0.510	—	-0.48	10
3661.352	0.041	-0.360	—	-0.45	10
3670.821	0.104	-0.240	—	-0.58	10
3706.752	0.485	-0.600	—	-0.50	10
3718.883	0.378	-0.310	—	-0.35	10
3731.263	0.104	-0.330	—	-0.70	10
3739.120	0.041	-0.430	—	-0.45	10
3743.877	0.333	-0.550	—	-0.21	10
3758.460	0.000	-1.102	—	-0.30	4
3760.710	0.185	-0.400	—	-0.48	10
3762.588	0.248	-0.850	—	-0.43	10
Eu II (Z=63)					
2906.669	0.000	-0.440	-0.75	—	11
Gd II (Z=64)					
2833.748	0.492	-0.096	-0.22	—	4
3358.625	0.032	0.250	—	-0.32	12
3360.712	0.032	-0.540	—	-0.33	12
3362.239	0.079	0.430	—	-0.30	12
3364.245	0.000	-1.086	—	-0.35	4
3392.527	0.079	-0.330	—	-0.25	12
3418.729	0.000	-0.360	—	-0.22	12
3422.464	0.240	0.710	—	-0.06	12
3423.924	0.000	-0.550	—	-0.34	12
3439.208	0.382	0.080	—	-0.36	12
3439.787	0.425	-0.120	—	-0.28	12
3439.988	0.240	0.210	—	-0.24	12
3451.236	0.382	-0.260	—	-0.32	12
3454.907	0.032	-0.640	—	-0.29	12
3463.990	0.427	0.250	—	-0.32	12

Table A.1. continued.

$\lambda(\text{\AA})$	χ_{ex} (eV)	log gf	A(X) _{STIS}	A(X) _{UVES}	Ref.
3467.274	0.425	0.080	—	-0.39	12
3473.224	0.032	-0.370	—	-0.23	12
3481.802	0.492	0.110	—	-0.35	12
3482.607	0.427	-0.470	—	-0.35	12
3491.960	0.000	-0.530	—	-0.25	12
3557.058	0.600	0.040	—	-0.28	12
3646.196	0.240	0.320	—	-0.39	12
3654.624	0.079	-0.080	—	-0.27	12
3656.152	0.144	-0.020	—	-0.36	12
3671.205	0.079	-0.220	—	-0.25	12
3699.737	0.354	-0.290	—	-0.37	12
3768.396	0.079	0.210	—	-0.25	12
3796.384	0.032	0.020	—	-0.22	12
Tb II (Z=65)					
2934.802	0.126	-0.596	-0.50	—	4
3509.144	0.000	0.700	—	-1.05	13
3633.287	0.641	0.090	—	-1.00	13
3641.655	0.649	0.040	—	-1.00	13
Dy II (Z=66)					
3407.796	0.000	0.180	—	-0.15	14
3413.784	0.103	-0.520	—	-0.16	14
3434.369	0.000	-0.450	—	-0.19	14
3454.317	0.103	-0.140	—	-0.16	14
3456.559	0.590	-0.110	—	-0.12	14
3460.969	0.000	-0.070	—	-0.14	14
3531.707	0.000	0.770	—	+0.15	14
3534.960	0.103	-0.040	—	-0.09	14
3536.019	0.538	0.530	—	-0.18	14
3546.832	0.103	-0.550	—	-0.11	14
3550.218	0.590	0.270	—	-0.22	14
3563.148	0.103	-0.360	—	-0.11	14
3694.810	0.103	-0.110	—	-0.08	14
Er II (Z=68)					
2897.518	1.654	0.573	-0.20	—	4
2904.468	0.846	0.330	-0.10	—	15
2964.520	0.846	0.580	-0.30	—	15
3364.076	0.055	-0.420	—	-0.40	15
3441.130	0.055	-0.580	—	-0.30	15
3499.103	0.055	0.290	—	-0.40	15
3524.913	0.000	-0.790	—	-0.40	15
3549.844	0.670	-0.290	—	-0.36	15
3559.894	0.000	-0.690	—	-0.45	15
3580.518	0.055	-0.620	—	-0.35	15
3616.566	0.000	-0.310	—	-0.14	15
3618.916	0.670	-0.500	—	-0.12	15
3633.536	0.000	-0.530	—	-0.46	15
3700.720	0.055	-1.290	—	-0.22	4
3729.524	0.000	-0.590	—	-0.29	15
3742.640	0.636	-0.360	—	-0.36	15
3786.836	0.000	-0.520	—	-0.34	15
Tm II (Z=69)					
3015.294	0.029	-0.590	-1.00	—	16
3131.255	0.000	0.080	—	-1.25	16
3362.615	0.029	-0.200	—	-1.00	16
3397.498	0.000	-0.810	—	-1.11	16
3462.197	0.000	0.030	—	-1.31	14
3700.256	0.029	-0.380	—	-1.18	14
3701.363	0.000	-0.540	—	-1.29	14
3761.914	0.000	-0.450	—	-1.22	16
3795.760	0.029	-0.230	—	-1.22	14
Lu II (Z=71)					

Table A.1. continued.

$\lambda(\text{\AA})$	χ_{ex} (eV)	log gf	A(X) _{STIS}	A(X) _{UVES}	Ref.
2847.505	1.463	-0.230	-1.03	—	17
2963.318	1.463	-0.240	-1.00	—	17
3077.605	1.542	0.160	—	-1.20	17
Hf II (Z=72)					
3012.900	0.000	-0.600	-0.77	—	18
3109.113	0.787	-0.260	—	-0.60	18
3255.279	0.452	-1.210	—	-0.55	18
3399.793	0.000	-0.570	—	-0.81	18
3569.034	0.787	-0.460	—	-0.90	18
Ta II (Z=73)					
2635.583	0.128	0.700	-2.15	—	4
2832.702	0.847	-0.070	-1.05	—	4
W II (Z=74)					
2697.706	0.188	-0.870	-0.90	—	4
Re I (Z=75)					
2930.613	1.867	2.000	-0.20	—	4
Re II (Z=75)					
2637.006	2.373	1.020	-0.21	—	4

References. (1) Biémont et al. (1999); (2) Hannaford et al. (1982); (3) Ljung et al. (2006); (4) VALD; (5) Biémont et al. (1981); (6) Sikström et al. (2001); (7) Wickliffe et al. (1994); (8) Lawler et al. (2009); (9) Den Hartog et al. (2003); (10) Lawler et al. (2006); (11) Zhiguo et al. (2000); (12) Den Hartog et al. (2006); (13) Lawler et al. (2001c); (14) Sneden et al. (2009); (15) Lawler et al. (2008); (16) Wickliffe & Lawler (1997); (17) Quinet et al. (1999); (18) Lawler et al. (2007)